Article

Cell Reports

Reduced Insulin/IGF-1 Signaling Restores the Dynamic Properties of Key Stress Granule Proteins during Aging

Graphical Abstract

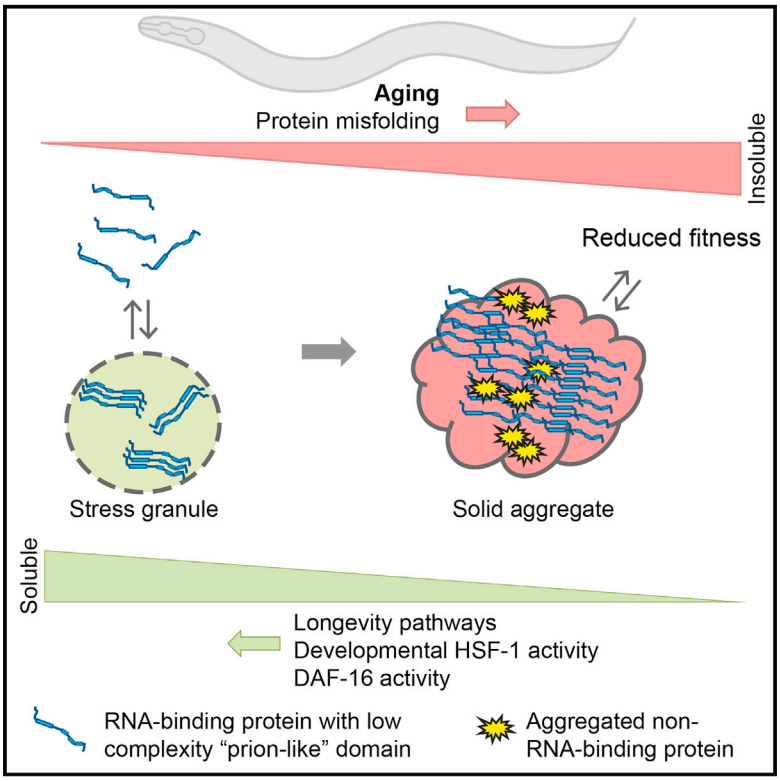

Authors

Marie C. Lechler, Emily D. Crawford, Nicole Groh, ..., Jonathan C. Trinidad, Alma L. Burlingame, Della C. David

Correspondence

della.david@dzne.de

In Brief

Lechler et al. show that RNA-binding proteins (RBPs) including stress granule proteins are prone to aggregate with age in *C. elegans*. Aggregation of stress granule RBPs with "prion-like" domains is associated with reduced fitness. Their aggregation is prevented by longevity pathways and promoted by the aggregation of other misfolded proteins.

Highlights

- RNA-binding proteins (RBPs) with "prion-like" domains form solid aggregates with age
- Reduced *daf-2* signaling preferentially prevents insolubility of RNA granule proteins
- Co-aggregation with other misfolded proteins promotes stress granule RBP aggregation
- Aggregation of key stress-granule-related RBPs is associated with impaired health

Accession Numbers

PXD003451

Lechler et al., 2017, Cell Reports *18*, 454–467
January 10, 2017
http://dx.doi.org/10.1016/j.celrep.2016.12.033

OPEN ACCESS
CellPress

Cell Reports
Article

Reduced Insulin/IGF-1 Signaling Restores the Dynamic Properties of Key Stress Granule Proteins during Aging

Marie C. Lechler,[1,2] Emily D. Crawford,[1,5] Nicole Groh,[1,2] Katja Widmaier,[1] Raimund Jung,[1] Janine Kirstein,[3] Jonathan C. Trinidad,[4,6] Alma L. Burlingame,[4] and Della C. David[1,7,*]

[1]German Center for Neurodegenerative Diseases, 72076 Tübingen, Germany
[2]Graduate Training Centre of Neuroscience, 72074 Tübingen, Germany
[3]Leibniz-Institut für Molekulare Pharmakologie im Forschungsverbund Berlin, 13125 Berlin, Germany
[4]Mass Spectrometry Facility, Department of Pharmaceutical Chemistry, University of California, San Francisco, San Francisco, CA 94158, USA
[5]Present address: Department of Biochemistry and Biophysics, University of California, San Francisco, San Francisco, CA 94158, USA
[6]Present address: Department of Chemistry, Indiana University, Bloomington, IN 47405, USA
[7]Lead Contact
*Correspondence: della.david@dzne.de
http://dx.doi.org/10.1016/j.celrep.2016.12.033

SUMMARY

Low-complexity "prion-like" domains in key RNA-binding proteins (RBPs) mediate the reversible assembly of RNA granules. Individual RBPs harboring these domains have been linked to specific neurodegenerative diseases. Although their aggregation in neurodegeneration has been extensively characterized, it remains unknown how the process of aging disturbs RBP dynamics. We show that a wide variety of RNA granule components, including stress granule proteins, become highly insoluble with age in *C. elegans* and that reduced insulin/insulin-like growth factor 1 (IGF-1) *daf-2* receptor signaling efficiently prevents their aggregation. Importantly, stress-granule-related RBP aggregates are associated with reduced fitness. We show that heat shock transcription factor 1 (HSF-1) is a main regulator of stress-granule-related RBP aggregation in both young and aged animals. During aging, increasing DAF-16 activity restores dynamic stress-granule-related RBPs, partly by decreasing the buildup of other misfolded proteins that seed RBP aggregation. Longevity-associated mechanisms found to maintain dynamic RBPs during aging could be relevant for neurodegenerative diseases.

INTRODUCTION

Young, healthy organisms strive to maintain their proteome in a functional state through the tight control of rates of protein synthesis, folding, and degradation. Extensive quality-control systems are set up throughout the cell to prevent and manage protein damage. As the organism ages, these control mechanisms become less efficient, leading to a disruption in protein homeostasis (Balch et al., 2008; David, 2012). Aging is the main risk factor for a variety of neurodegenerative diseases where specific proteins accumulate as pathological aggregates. Recently, there has been considerable interest in investigating widespread protein aggregation in the absence of disease. Multiple studies have demonstrated that several hundred proteins become highly detergent-insoluble in aged animals (Ayyadevara et al., 2016; David, 2012; David et al., 2010; Demontis and Perrimon, 2010; Reis-Rodrigues et al., 2012; Tanase et al., 2016; Walther et al., 2015). Computational analysis of the insoluble proteome indicates an overrepresentation of proteins with functional and structural similarities (David et al., 2010). The examination of some of these proteins in vivo reveals their assembly into large "solid" aggregates with age similar to those formed in the context of disease. The discovery of endogenous age-dependent protein aggregation in model organisms gives us the unprecedented opportunity to dissect the intrinsic cellular machineries responsible for preventing protein aggregation without using ectopically expressed human disease-associated proteins. At this time, very little is known concerning the regulation of widespread protein insolubility with age and its consequences for the health of the organism. Interestingly, several studies show that protein insolubility is modified in long-lived animals with reduced insulin/insulin growth factor (IGF)-1 *daf-2* signaling, but it remains unclear to which extent (David et al., 2010; Demontis and Perrimon, 2010; Walther et al., 2015).

A growing number of familial and sporadic forms of neurodegenerative diseases show pathological inclusions caused by abnormal aggregation of RNA-binding proteins (RBPs). The first RBPs identified in these inclusions were TAR DNA binding protein of 43 kDa (TDP-43) and fused in sarcoma (FUS), associated with amyotrophic lateral sclerosis (ALS) and frontotemporal lobar degeneration (FTLD) (Arai et al., 2006; Neumann et al., 2009; Neumann et al., 2006). Since then additional RBPs such as TAF15, EWSR1, hnRNPA2B1, hnRNPA1,

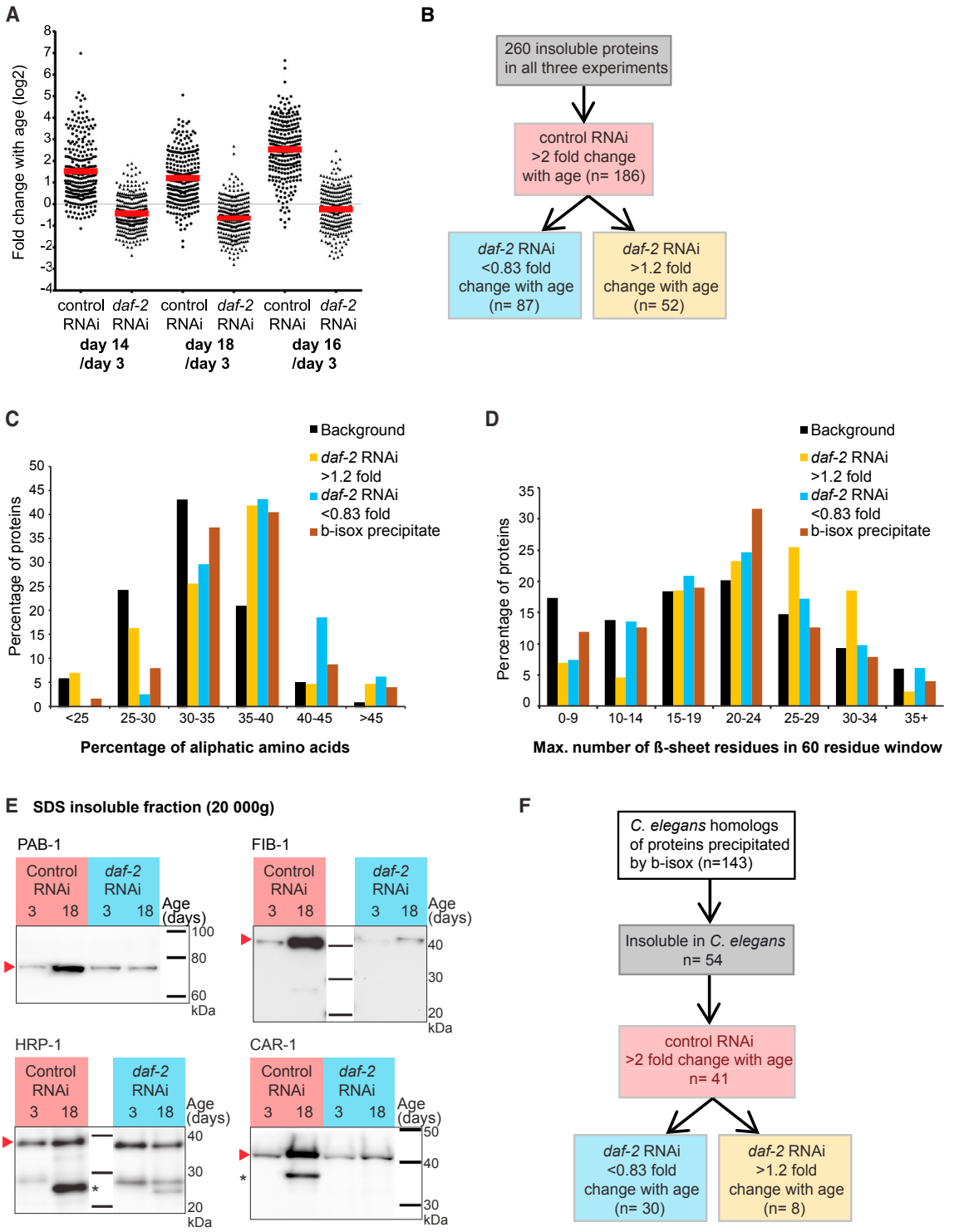

Figure 1. RNA Granule Components No Longer Aggregate in Long-Lived Animals with Reduced *daf-2* Signaling

(A) Distribution of fold changes with age in insolubility for 260 proteins (n = 3, biological replicates). Fold changes are measured by iTRAQ quantification.

(B) Flowchart describing the segregation of insolubility fold changes with age into different groups for analysis.

(C) Proteins with reduced aggregation in *daf-2* RNAi conditions and U2OS proteins precipitated by b-isox are enriched in aliphatic amino acids. Unequal variance t test: proteins aggregating more with age in long-lived animals (n = 43, >1.2-fold), p = 0.04; proteins aggregating less with age in long-lived animals (n = 81, <0.83-fold), p = 6.1E-15; proteins precipitated by b-isox (n = 126), p = 1.3E-9.

(legend continued on next page)

and hnRNPA3 have been associated with neurodegenerative diseases (Kim et al., 2013; Neumann et al., 2011). All of the known RBPs associated with dementia contain a low-complexity (LC) "prion-like" domain enriched in glycines and uncharged polar amino acids, and similar to the sequences driving yeast prion aggregation (Alberti et al., 2009; King et al., 2012). Mutations in this domain enhance pathology by accelerating aggregation (Johnson et al., 2009; Kim et al., 2013). LC prion-like domains are also present in key RBPs that mediate the assembly of RNA granules by liquid-liquid phase separation (Lin et al., 2015; Molliex et al., 2015; Murakami et al., 2015; Patel et al., 2015). Significantly, a small proportion of liquid droplets made by RBPs transform into solid aggregates over time in vitro (Lin et al., 2015; Molliex et al., 2015; Murakami et al., 2015; Patel et al., 2015). For clarity, we will use the term *aggregation* only when referring to the formation of non-dynamic RBP aggregates. An important question is whether the special assembly properties of RBPs puts them at risk of aggregating during aging in a multicellular organism and not just in the context of disease. Interestingly, several RBPs with LC prion-like domains were identified in the insoluble proteome of aged animals (David et al., 2010). Overall, it is imperative to know the causes and consequences of wild-type RBP aggregation during aging in order to fully understand RBP aggregation in neurodegenerative diseases. Furthermore, it is likely that the organism has evolved specific mechanisms to control liquid droplet protein aggregation.

In the current study, we chose to focus on key RBPs responsible for stress granule formation. Stress granules are a specific type of RNA granule that protect the cell by sequestering mRNA from the translational machinery during periods of stress. Importantly, stress granule proteins are often found to co-localize with pathological inclusions of TDP-43 and FUS (Bentmann et al., 2013; Li et al., 2013). Whether these stress granule proteins are innocent bystanders transiently interacting with TDP-43 and FUS or whether they co-aggregate and accelerate disease-associated RBP aggregation remains intensely debated (Bentmann et al., 2013; Li et al., 2013).

We show that key stress-granule-related RBPs (sgRBPs) accumulate in aberrant stress granule-like puncta and in large solid aggregates in aged *C. elegans*. Proteomic analysis revealed that long-lived animals with reduced *daf-2* signaling preferentially abrogate the insolubility of RNA granule components. Importantly, sgRBP aggregates are associated with reduced animal size, motility, and lifespan. We show that sgRBP aggregation is triggered at an earlier age by their co-aggregation with other misfolded proteins, a process that is prevented by DAF-16 in *daf-2* mutants. In addition, the proteostasis network established by heat shock transcription factor 1 (HSF-1) during development is required to maintain dynamic stress granule proteins throughout the animal's life.

RESULTS

Long-Lived Animals with Reduced *daf-2* Signaling Prevent Widespread Protein Insolubility with Age

To identify and quantify changes in aggregation-prone proteins in animals with reduced *daf-2* signaling, we performed an in-depth proteomic analysis of the insoluble proteome from both control and long-lived animals (Figure 1A; Table S1). Because protein misfolding and aggregation is highly abundant in aged *C. elegans* gonads and masks changes in other somatic tissues (David et al., 2010; Goudeau and Aguilaniu, 2010; Zimmerman et al., 2015), we used a gonad-less mutant to focus our analysis on protein insolubility in non-reproductive tissues. We isolated large aggregates that are pelleted by low centrifugal forces (20,000 × *g*) and insoluble in 0.5% SDS. In three biological replicates, we identified 260 insoluble proteins, of which 186 were highly prone to aggregate with age in control animals (Figure 1B). The strong correlations between the control replicates ($r = 0.77$, $r = 0.85$, and $r = 0.67$) and long-lived replicates ($r = 0.87$, $r = 0.86$. and $r = 0.82$) attest to the quality of the quantification and experimental reproducibility (Figures S1A and S1B). None of these insoluble proteins was more prone to aggregate with age in the long-lived animals as compared with controls. These results are consistent with previous observations (David et al., 2010; Demontis and Perrimon, 2010). Surprisingly, a recent proteomic study showed that endogenous protein insolubility is higher in *daf-2* mutants than in wild-type animals (Walther et al., 2015). To account for procedural differences, we performed the extraction following the less stringent extraction protocol from Walther et al. (2015). By omitting SDS and using ultracentrifugation at 500,000 × *g*, Walther et al. analyzed highly insoluble large aggregates (as in this study), as well as smaller and more soluble aggregates. However, we did not observe a general change in the action of *daf-2* signaling on protein insolubility with age after using the less stringent extraction protocol (Figure S1C). Next, we asked whether the inconsistencies between the studies could be related to protein aggregation in the gonad and indeed, we found that long-lived animals with gonads have proportionally more insoluble proteins compared with wild-type animals with gonads (Figure S1D). These results suggest that aggregation in the gonad masks the protective effect of reduced *daf-2* signaling in somatic tissues. Importantly, we confirmed this protective action of reduced *daf-2* signaling with several candidates (see below).

Taken together, these data demonstrate that reduced *daf-2* signaling promotes protein solubility in most tissues with age.

(D) Proteins that aggregate in both control and *daf-2* RNAi conditions are enriched in extended stretches of β-sheet propensity. Unequal variance t test: proteins aggregating more with age in long-lived animals (n = 43, >1.2-fold), p = 0.002; proteins aggregating less with age in long-lived animals (n = 81, <0.83-fold), p = 0.09; proteins precipitated by b-isox (n = 126), p = 0.6.

(E) Large SDS-insoluble aggregates precipitated by 20,000 × *g*. Immunoblots detecting RBPs PAB-1, FIB-1, HRP-1 (unspecific band noted by asterisk), and CAR-1 (truncated band marked by asterisk). Relevant protein bands are indicated by red arrow.

(F) Flowchart showing a high overlap between proteins precipitated by b-isox and aggregation-prone proteins in *C. elegans*, in particular those no longer aggregating in *daf-2(–)* conditions.

See also Figures S1, S2, and S3 and Tables S1, S2, S3, and S4.

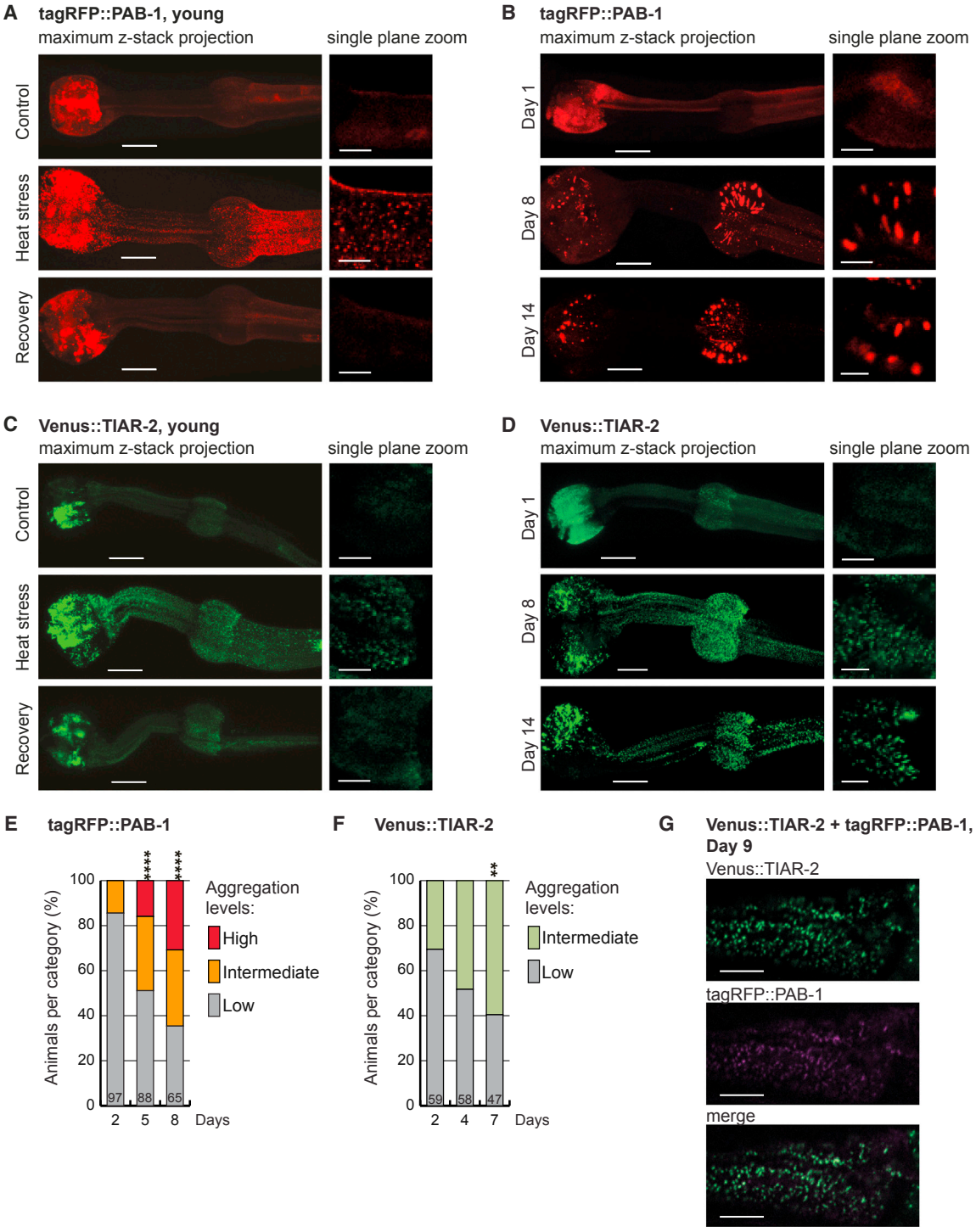

Figure 2. Stress-Granule-Related RBPs PAB-1 and TIAR-2 Aggregate with Age in *C. elegans*

(A) tagRFP::PAB-1 expressed in the pharyngeal muscles forms stress granules upon heat stress (2 hr, 32°C) on day 1 of adulthood. No stress granules are visible after recovery (+24 hr). Scale bars: z stack projection, 15 μm; single-plane insets, 5 μm.

(B) tagRFP::PAB-1 distribution changes from a diffuse pattern in young animals to a punctate pattern in aged worms. Scale bars: z stack projection, 15 μm; single-plane insets, 5 μm.

(C) Venus::TIAR-2 expressed in the pharyngeal muscles forms stress granules upon heat stress (2 hr, 32°C) on day 1 of adulthood. No stress granules are visible after recovery (+24 hr). Scale bars: z stack projection, 15 μm; single-plane insets, 5 μm.

(D) Venus::TIAR-2 accumulates mainly in stress-granule-like puncta with age. Scale bars: z stack projection, 15 μm; single-plane insets, 5 μm.

(legend continued on next page)

Reduced *daf-2* Signaling Preferentially Abrogates the Insolubility of RNA Granule Components

To investigate specifically changes in insolubility regulated by reduced *daf-2* signaling, we sorted proteins prone to aggregate with age in control animals (>2-fold) by their fold change in insolubility with age in the long-lived conditions. We restricted our analysis to 87 proteins that aggregated less with age (<0.83-fold) and 52 proteins that continued to aggregate with age (>1.2-fold) in the long-lived animals (Figure 1B; Table S1). Previous bioinformatics analysis of aggregation-prone proteins revealed an enrichment in both β-sheet propensity and aliphatic amino acids (David et al., 2010). A similar enrichment in the whole insoluble proteome was identified in this study (Figures S1E and S1F). Intriguingly, when examining the two groups of insoluble proteins that were differentially regulated by reduced *daf-2* signaling, we found a segregation of the two properties. Proteins with abrogated aggregation with the *daf-2* RNAi treatment were highly enriched in aliphatic amino acids, in particular alanine, glycine, and valines, but not in β sheets (Figures 1C, 1D, and S1G). Conversely, proteins that still aggregate in the *daf-2(−)* condition had a significant propensity to form β sheets but were only modestly enriched in aliphatic amino acids (Figures 1C and 1D).

Next, we searched for functional differences between the two groups differentially regulated by reduced *daf-2* signaling. Strikingly, ribosomal proteins and RNA granule components, including stress granule and P-granule RBPs, were highly overrepresented among the proteins that were prevented from aggregating with age in the long-lived animals (Tables S2A and S3). Conversely, chaperones and vitellogenin yolk proteins were overrepresented among proteins that were still prone to aggregate with age in *daf-2(−)* conditions (Table S2B). Among the RBPs, four are predicted to have LC prion-like domains (Alberti et al., 2009): PAB-1, FIB-1, HRP-1, and CAR-1 (Figure S2A). By western blot, we confirmed that reduced *daf-2* signaling abrogated their aggregation with age (Figures 1E and S2B). In addition, we evaluated two proteins without RNA-binding or LC prion-like domains, PAR-5 and DAF-21, quantified by mass spectrometry as more insoluble with age in both control and long-lived animals. We confirmed that PAR-5 and DAF-21 continued to aggregate with age in long-lived animals (by >7-fold and 10-fold, respectively), albeit to a reduced extent compared with controls (Figure S2C). Of note, changes in aggregation were not correlated with changes in total protein levels (Figure S3).

A previous study found that the chemical b-isox exclusively causes RNA granules to precipitate out from whole-cell lysates by inducing their assembly into a hydrogel (Han et al., 2012; Kato et al., 2012). Proteins precipitated by b-isox were also enriched in aliphatic amino acids (in particular glycine and to a lesser extent alanine and valine) and not in the propensity to form β sheets (Figures 1C, 1D, and S1G). We checked for proteins in common with our study and found a very significant overlap between proteins precipitated by b-isox and proteins no longer aggregating in the long-lived conditions (Figure 1F; Table S4).

Together, these results indicate that different types of RNA granule components including key RBPs responsible for their assembly become insoluble with age, and long-lived animals with reduced *daf-2* signaling are highly successful in preventing their aggregation. Interestingly, higher levels of aliphatic amino acids in RNA granule components could help their assembly and/or drive their age-dependent aggregation.

Key Stress Granule Proteins PAB-1 and TIAR-2 Form Solid Aggregates in Aged *C. elegans*

To investigate further the aggregation of key RBPs with LC prion-like domains and to understand the mechanisms involved, we generated *C. elegans* strains expressing PAB-1 and TIAR-2 in the pharyngeal muscles, fused to fluorescent tags. PAB-1 and TIAR-2 are the *C. elegans* homologs of human polyadenylate-binding protein 1 (PABP-1) and T-cell-restricted intracellular antigen-1 (TIA-1), two prominent RBPs that localize to stress granules and are also minor components of pathological inclusions that occur in ALS and FLTD (Bentmann et al., 2012). Both of these RBPs harbor LC prion-like domains (Figure S2A) (Alberti et al., 2009).

Exposing cells to stressors such as heat induces RBPs with LC prion-like domains to form liquid droplets (Molliex et al., 2015; Patel et al., 2015). Similarly, heat shock in *C. elegans* caused PAB-1 and TIAR-2 to form stress granules (Figures 2A and 2C; Figure S4A) (Murakami et al., 2012; Rousakis et al., 2014). When co-expressed, PAB-1 and TIAR-2 localized to the same stress granules (Figure S4B). Consistent with the dynamic nature of stress granules, these puncta were no longer observed 24 hr after the heat shock (Figures 2A and 2C). Using antibodies, we observed a similar change in pattern with endogenous PAB-1, indicating the effect is not merely due to overexpression or the fluorescent tag (Figure S4C). As an additional control, we showed that kinase KIN-19, which is not an RBP and lacks a LC prion-like domain, does not localize to stress granules upon heat shock (Figure S4D).

With age, we observed a striking change in the distribution pattern of these key stress granule RBPs. Whereas the majority of PAB-1 and TIAR-2 proteins were diffusely localized in non-stressed young animals, we found that both stress granule components accumulated in distinct puncta in aged animals (Figures 2B and 2D; Figure S4F). This change was specific for PAB-1 and TIAR-2 as the fluorescent tags alone (Venus or tagRFP) remained diffuse with age (Figure S4E) (David et al., 2010). The results were not simply caused by overexpression because endogenous PAB-1 formed similar puncta with age, in the different head regions where it is natively expressed (Figure S4G). For both PAB-1 and TIAR-2, we observed a significant increase with

(E) Increased tagRFP::PAB-1 aggregation with age in a population of *C. elegans*. Day 5 or 8 versus day 2: ****$p < 0.0001$.
(F) Increased Venus::TIAR-2 aggregation with age in a population of *C. elegans*. Day 7 versus day 2: **$p < 0.01$.
(G) tagRFP::PAB-1 co-localizes with stress-granule-like Venus::TIAR-2 puncta in double-transgenic animals. Representative single-plane images. Scale bar, 7 μm.
See also Figure S4.

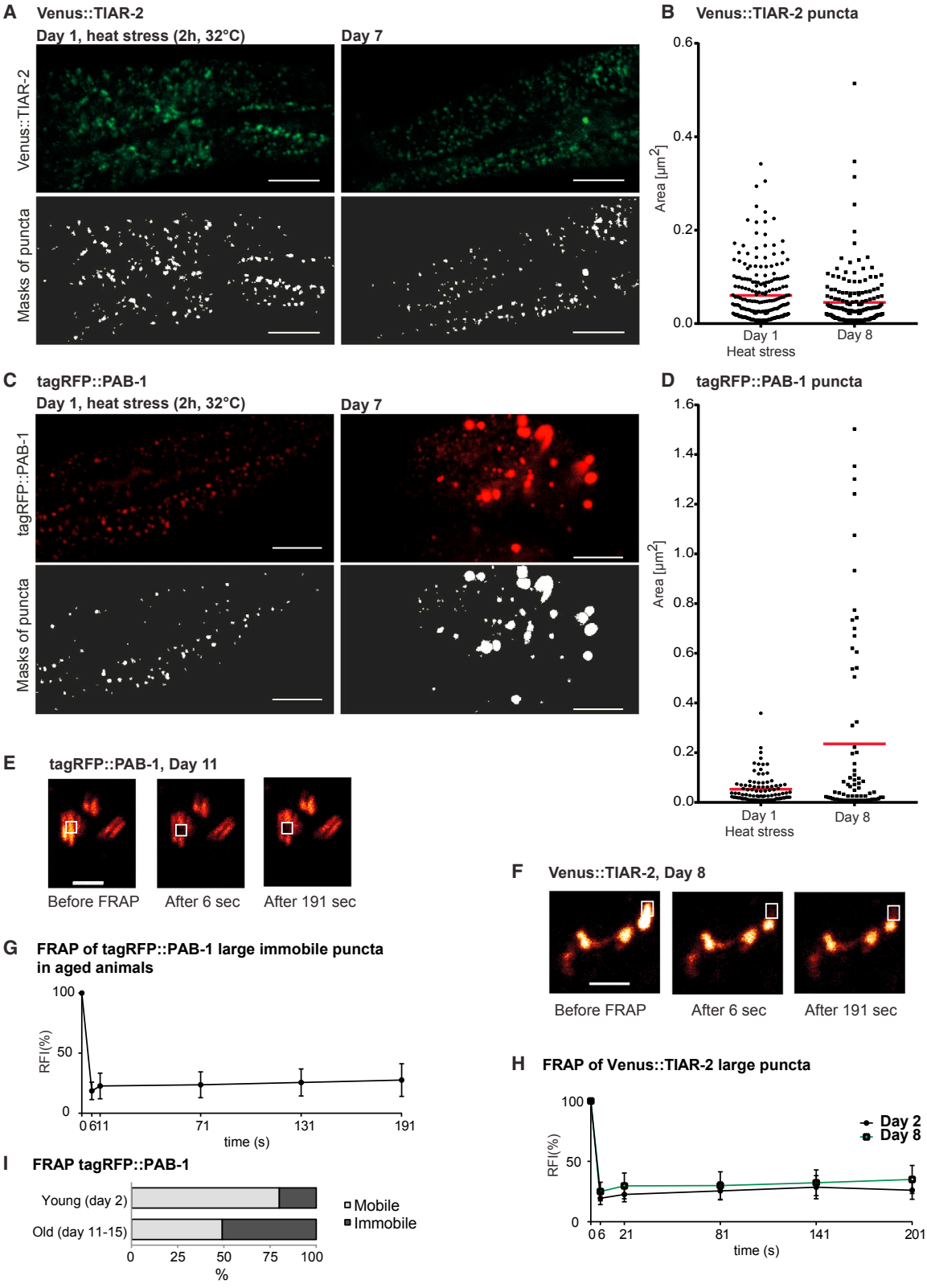

(legend on next page)

age in the number of worms with large puncta that are visible by low-magnification microscopy (Figures 2E and 2F; Figure S4H). Interestingly, imaging at high magnification revealed that TIAR-2 in aged animals was localized predominantly in small puncta highly reminiscent of stress granules assembled during heat shock, whereas PAB-1 accumulated to a greater extent in large puncta that were not normally observed upon heat shock in young animals (Figures 2B, 2D, single-plane insets, 3A, 3C, and 3D). Quantification confirmed that stress granules induced during heat shock and aberrant TIAR-2 stress granule-like puncta formed during aging had similar sizes (Figure 3B). Remarkably, when co-expressed, PAB-1 preferentially co-localized within TIAR-2-positive age-dependent stress-granule-like puncta (Figure 2G), suggesting that interactions between RBPs change their aggregation patterns.

A hallmark of protein aggregation associated with disease is the immobility of proteins within the aggregates. To evaluate this aspect, we monitored fluorescence recovery after photobleaching (FRAP) in large PAB-1 and TIAR-2 puncta (Figures 3E–3I). All large TIAR-2 puncta and half of the large PAB-1 puncta in aged animals showed no fluorescence recovery, demonstrating that these are solid aggregates (Figures 3E–3I). Because of the small size of the age-dependent stress-granule-like puncta, it was not possible to assess the mobility of TIAR-2 or PAB-1 in these structures. Consequently, we used the large puncta as a readout for sgRBP aggregation in subsequent experiments.

Aggregation of Key Stress Granule Component PAB-1 Is Associated with Reduced Fitness

The consequences of age-dependent protein aggregation for the animal's health are poorly understood. Here, we evaluated the impact of the aggregation of a key stress granule component during aging. Surprisingly, PAB-1 overexpression was protective as animals, grown at 15°C, 20°C, or 25°C all their life, lived longer than non-transgenic animals (Table S5). However, this effect is likely due to higher levels of functional PAB-1 and not related to protein aggregation because PAB-1 does not aggregate in animals at 15°C (Figure S5A). In order to distinguish effects specifically related to PAB-1 aggregation, we separated PAB-1 transgenics at day 7 into three groups depending on their aggregation levels. We found that animals with PAB-1 aggregation were significantly smaller in size compared with animals without PAB-1 aggregation (Figure 4A; Figure S5B). In addition, smaller animals were visibly less motile (Movie S1). Importantly, mildly stressed animals with the highest levels of aggregation died earlier (Figure 4B; Table S5). Overall, these results demonstrate that PAB-1 aggregation is associated with impaired health.

HSF-1 Activity during Development Protects against sgRBP Aggregation

Our proteomic study revealed that reduced *daf-2* signaling efficiently prevents the insolubility of stress granule components with age. We confirmed that long-lived *daf-2* mutants greatly delay the formation of both stress-granule-like structures and large aggregates of PAB-1 and TIAR-2 (Figures 5A and 5B; Figures S6A and S6B). To gain insight into the mechanisms controlling protein aggregation, we investigated the role of the transcription factor HSF-1 activated by reduced *daf-2* signaling (Hsu et al., 2003; Volovik et al., 2012). Chaperones HSP110, HSP70, and HSP40 modulate stress granule dynamics in *Saccharomyces cerevisiae* and/or in cell culture (Cherkasov et al., 2013; Gilks et al., 2004; Kroschwald et al., 2015; Walters et al., 2015). Because chaperone expression is controlled by HSF-1 in *C. elegans*, we speculated that HSF-1 may regulate sgRBP aggregation. Indeed, impairing HSF-1 activity in both *daf-2(−)* and wild-type backgrounds caused severe PAB-1 aggregation already in young adults as well as in aged individuals, an effect that was reversed by overexpressing HSF-1 (Figures 5C–5E; Figures S6C and S6D). Interestingly, HSF-1 in *daf-2* mutants did not control the aggregation of the kinase KIN-19, which was previously shown to misfold and form solid aggregates with age (Figure 5G) (David et al., 2010). These results suggest that HSF-1 regulates different types of endogenous protein aggregation with age to different extents. It was previously shown that to assure *daf-2(−)* longevity, HSF-1 is most highly expressed and acts mainly during development (Volovik et al., 2012). We observed that impairing HSF-1 activity by RNAi during adulthood had no effect on PAB-1 aggregation (Figure 5F; Figure S6E). Conversely, reducing HSF-1 activity by RNAi during development caused PAB-1 aggregation in young adults, albeit mainly in the anterior bulb (Figure 5F).

Figure 3. TIAR-2 and PAB-1 Accumulate in Stress-Granule-like Puncta and Large Immobile Puncta in Aged *C. elegans*

(A) Small Venus::TIAR-2 puncta formed with age are similar to stress granules formed during heat stress. Representative single-plane images and masks of puncta for size quantification. Scale bars, 5 μm.

(B) Size quantification of Venus::TIAR-2 puncta from masks of representative single-plane images in (A).

(C) Representative single-plane images and masks of puncta for size quantification showing large tagRFP::PAB-1 puncta formed with age compared with stress granules assembled during heat stress. Scale bars, 5 μm.

(D) Size quantification of tagRFP::PAB-1 puncta from masks of representative single-plane images in (C). Puncta larger than 0.5 μm^2 were considered as "large" puncta.

(E) Representative immobile tagRFP::PAB-1 puncta at day 11 assayed by FRAP. Bleached area is marked by white box. Scale bar, 4 μm.

(F) Representative immobile Venus::TIAR-2 puncta at day 8 assayed by FRAP. Bleached area is marked by white box. Scale bar, 2 μm.

(G) FRAP analysis of immobile tagRFP::PAB-1 puncta present in aged worms (days 11–12). Quantification of relative fluorescence intensity (RFI) over time. Number of animals = 6, puncta evaluated = 6, mean ± SD is represented.

(H) Venus::TIAR-2 puncta monitored by FRAP were highly immobile both in young (day 2) and in aged (day 8) animals. In both young and aged animals: animals = 5, puncta evaluated = 5, mean ± SD is represented.

(I) Quantification of FRAP results shows increased immobility of tagRFP::PAB-1 puncta with age. Twenty percent of tagRFP::PAB-1 puncta present in young worms (day 2) were immobile (number of animals = 18, puncta evaluated = 57) compared with 51% in aged worms (days 11–15) (number of animals = 18, puncta evaluated = 55).

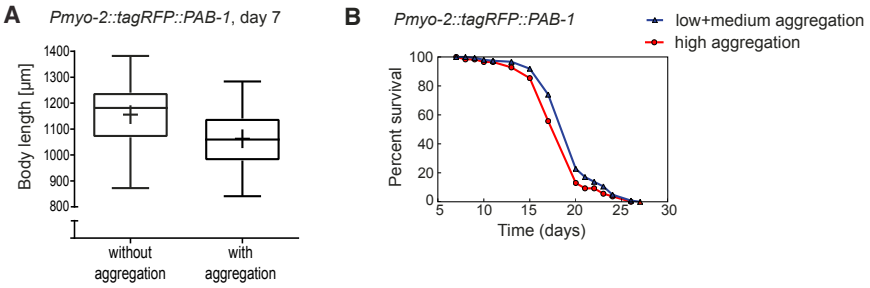

Figure 4. Aggregation of Stress Granule Component PAB-1 with Age Is Associated with Reduced Fitness

(A) Animals with tagRFP::PAB-1 aggregation are significantly smaller than animals without aggregation (day 7, $p < 0.0001$). Data are represented with Tukey-style box plots and mean indicated by + (animals without aggregation n = 99, with aggregation n = 125). See also Figure S5B.

(B) High levels of tagRFP::PAB-1 aggregation are associated with reduced survival. Survival curve of *Pmyo-2::tagRFP::PAB-1* animals grown at 20°C until day 7, sorted by their aggregation levels at day 7, and then transferred to 25°C (repeat 1: $p = 0.029$; see Table S5).

See also Figure S5, Table S5, and Movie S1.

The same chaperones discovered to regulate stress granule dynamics in other model systems could also play a role in preventing sgRBP aggregation. In yeast the Hsp40 proteins Sis1 and Ydj1 were shown to co-localize with stress granules and to play a role in stress granule disassembly (Walters et al., 2015). We evaluated worm strains overexpressing yellow fluorescent protein (YFP)-tagged DNJ-13 and DNJ-19, the worm orthologs of Sis1 and Ydj1, together with tagRFP::PAB-1. We observed occasional co-localization of both chaperones with both heat-induced PAB-1 stress granules and age-dependent large and stress-granule-like PAB-1 puncta (Figures S6G and S6H). These findings were confirmed in single tagRFP::PAB-1 transgenics using antibodies against DNJ-13 and DNJ-19 (data not shown). However, overexpression of DNJ-19 and DNJ-13 did not significantly reduce PAB-1 aggregation with age (Figures S6F and S6I), indicating that these chaperones may not modulate sgRBP aggregation. In addition, we performed immunostaining for HSP110. However, we observed no co-staining with either PAB-1 stress granules induced by heat shock or PAB-1 puncta formed during aging. Therefore, it is possible that HSP110 does not modulate stress granule dynamics and sgRBP aggregation in *C. elegans*. Finally, we investigated the role of HSP70 on sgRBP aggregation and found that inhibition of HSP70 by RNAi did not alter PAB-1 aggregation (Table S6). Of note, the later results could be caused by redundancy between chaperone functions.

Collectively, these results reveal that HSF-1 is an important regulator of sgRBP aggregation throughout life, and it contributes to maintaining dynamic stress granule proteins in long-lived *daf-2* mutants. The exact chaperones responsible for preventing sgRBP aggregation remain to be determined.

daf-2 Mutants Avoid sgRBP Aggregation in Part by Eliminating Putative Cross-Seeding

Next, we examined the role of the transcription factor DAF-16 activated by reduced *daf-2* signaling (Lin et al., 1997; Ogg et al., 1997). In *daf-2* mutants, DAF-16 protected against PAB-1 aggregation in aged animals (Figures 5C and 5D). Importantly, *daf-2* mutants use DAF-16 to control different types of age-dependent protein aggregation because delayed aggregation of the kinase KIN-19 was also dependent on DAF-16 (Figure 5G).

Recent work performed in *S. cerevisiae* and *Drosophila* reveals that stress granules dynamically interact with misfolded proteins (Cherkasov et al., 2013; Kroschwald et al., 2015). We speculated that widespread protein misfolding and aggregation occurring with age could promote sgRBP aggregation. In support of this hypothesis, we observed the co-localization of PAB-1 and KIN-19 in large immobile aggregates in double transgenics (Figures 6A and 6B). Next, we evaluated the rate of PAB-1 and KIN-19 aggregation in the double transgenics relative to their aggregation rates in single transgenics (Figures 6C and 6D). In the single transgenics, KIN-19 aggregated faster and to a greater extent than PAB-1. Importantly, when both PAB-1 and KIN-19 were co-expressed, the presence of misfolded KIN-19 triggered more abundant PAB-1 aggregation at an earlier age (Figure 6C). Conversely, KIN-19 aggregation was slightly impeded by PAB-1 overexpression (Figure 6D), indicating that sgRBP aggregation does not cross-seed KIN-19 aggregation. Notably, PAB-1 aggregation was not accelerated by the co-expression of a fluorescent tag alone (Figure 6E). Furthermore, we did not observe a general induction of PAB-1 stress granules in young double-transgenic animals expressing both KIN-19 and PAB-1 (Figure S6J). These data strongly suggest that PAB-1 aggregation is not simply the consequence of generalized cellular stress induced by KIN-19 overexpression. Rather, the co-localization of KIN-19 and PAB-1 in the same aggregates as well as the earlier and accelerated aggregation of PAB-1 is consistent with a seeding mechanism related to KIN-19 aggregation.

Taken together, we interpret these findings to imply that the accumulation of misfolded proteins with age acts as a seed for sgRBP aggregation. Therefore, the overall reduction in widespread protein aggregation in long-lived *daf-2(–)* conditions as evidenced by our proteomic analysis, at least in part through increased DAF-16 activity, could be an effective strategy to prevent sgRBP aggregation.

Other Longevity Pathways Prevent Age-Dependent sgRBP Aggregation

Several experimental manipulations have been shown to extend the lifespan of *C. elegans* and protect against proteotoxicity (Kenyon, 2010; Taylor and Dillin, 2011). We wondered whether other pathways extending lifespan could also protect against sgRBP aggregation. We found that both dietary restriction mimicked in *eat-2* mutant animals as well as inhibition of mitochondrial function achieved by targeting *cyc-1* with RNAi strongly limited PAB-1 aggregation with age (Figures 7A and

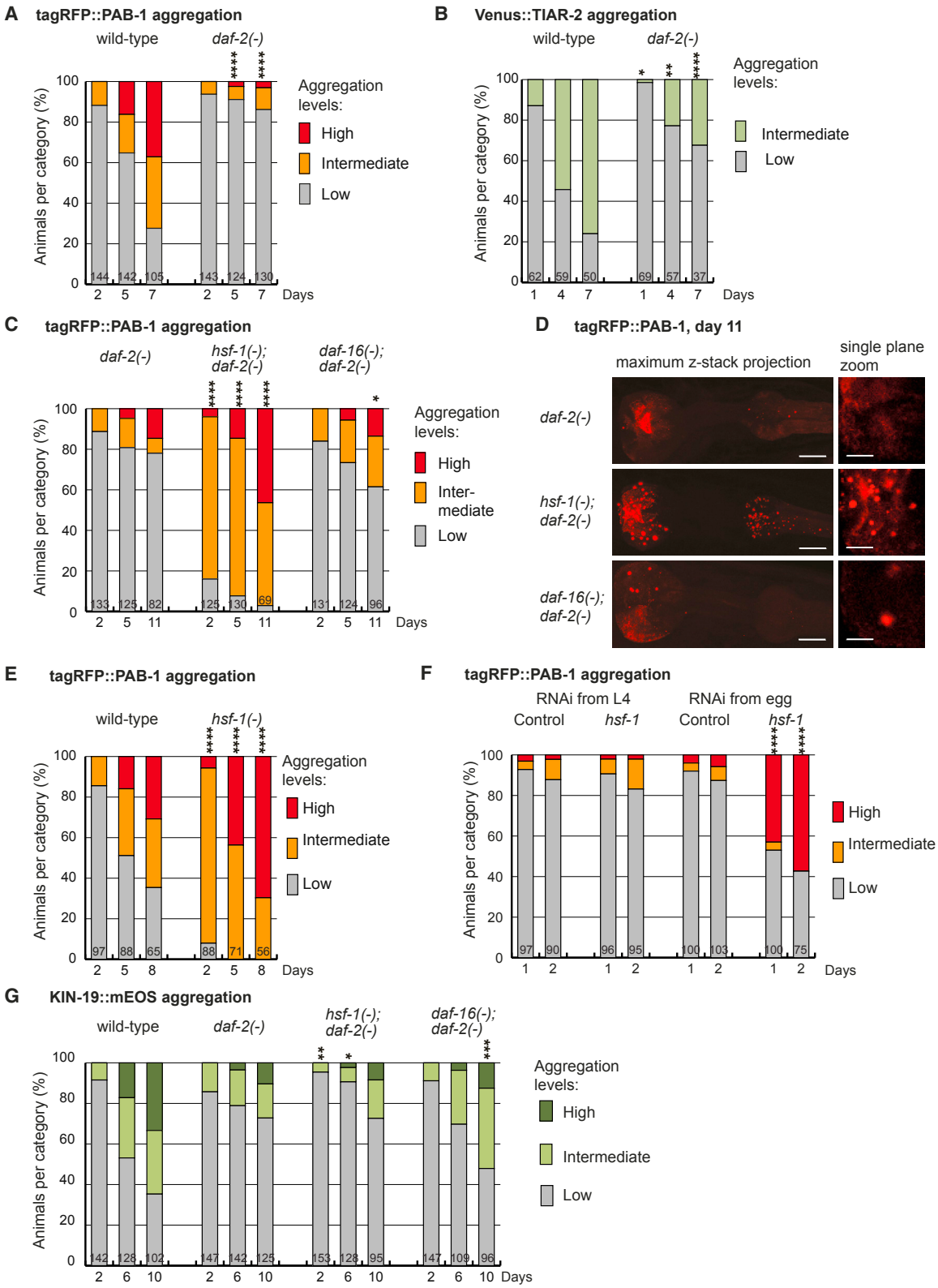

(legend on next page)

7B). Therefore, maintaining dynamic RBPs could be a common strategy associated with longevity.

DISCUSSION

We show that a wide variety of RNA granule components become highly insoluble with age in *C. elegans*. Together with previous in vitro and cell culture results, our findings demonstrate that the capacity of RBPs to cycle between assembled and disassembled states can become a liability in aging organisms. Already in young animals, maintaining sgRBP dynamics necessitates an active control system established by HSF-1. The accumulation of other misfolded proteins during age acts as a seed for the aggregation of key sgRBPs. Significantly, one of the main outcomes of the longevity program initiated by reduced *daf-2* signaling while responding to widespread protein aggregation is the preservation of RBP solubility with age.

In this study, we have examined in detail the aggregation pattern of PAB-1 and TIAR-2, two key RBPs with LC prion-like domains that are important for the formation of stress granules. During the aging process, both proteins spontaneously assembled into small puncta similar to liquid droplets induced during stress and into larger aggregates. Significantly, upon co-expression, both PAB-1 and TIAR-2 co-localized in these age-related stress-granule-like structures. Because our proteomic analysis revealed a number of stress granule components in the insoluble proteome, it is likely that secondary stress granule proteins are also incorporated. Therefore, an attractive hypothesis is that these small puncta represent stress granules formed as a response to stress related to aging. The inherent aggregation propensity of sgRBPs would induce at least some of these droplets to undergo the irreversible transition into a solid state. These stabilized stress granules could then grow into large aggregates as we observed with PAB-1, or simply accumulate with age as seen with TIAR-2.

An important question remains how the inherent propensity of RNA granule components to aggregate with age could influence pathogenesis in neurodegenerative diseases.

One possibility is that inherent RBP aggregation impacts cellular health and thereby indirectly accelerates pathology. We observed reduced lifespan and a striking decrease in size and mobility of animals with higher levels of PAB-1 aggregation. As yet, it remains unclear whether reduced fitness is a cause or consequence of PAB-1 aggregation. In support of a gain of function related to sgRBP aggregation, two rare diseases are caused by mutated PABPN1 and TIA-1, the human homologs of PAB-1 and TIAR-2, which accumulate in pathological aggregates (Brais et al., 1998; Klar et al., 2013). Our proteomic analysis of aging *C. elegans* highlighted three other RBPs with LC prion-like domains that are highly prone to aggregate with age: HRP-1, FIB-1, and CAR-1. The aggregation of the human homologs of HRP-1, hnRNP-A1, and hnRNP-A3 was recently discovered to cause multisystem proteinopathy and ALS/FTLD (Kim et al., 2013; Mori et al., 2013). The aggregation of both FIB-1 and CAR-1 could also be detrimental. Indeed, a loss in nucleolar protein FIB-1 function caused by its aggregation with age could impair ribosomal biogenesis (Tollervey et al., 1991). The mammalian LSM14B and LSM14A homologs of CAR-1 localize to P bodies (Eulalio et al., 2007), and aggregation of key P-body components could impair non-sense-mediated decay. Therefore, it will be important to investigate the consequences of FIB-1 and CAR-1 aggregation on cellular health.

Apart from accelerating pathology indirectly by reducing cellular health, aggregating RBPs could directly influence pathological protein aggregation. The presence of stress granule proteins in pathological protein aggregates is emerging as a common denominator in different types of neurodegenerative diseases including ALS, FTLD, Alzheimer's disease, and Huntington's disease (Aulas and Vande Velde, 2015; Bentmann et al., 2013). The inherent aggregation propensity of stress granule proteins demonstrates that they are unlikely to be transient interacting partners in pathological aggregates. It remains to be determined whether age-related sgRBP aggregation acts as a seed for disease-associated protein aggregation. Overall, the role of stress granules in neurodegenerative diseases is clearly highly complex because there is evidence supporting the recruitment of disease-associated proteins to stress granules and vice versa. Interestingly, recent cell culture data show that the assembly of stress granules caused by disease-associated protein aggregation in turn promotes pathological aggregation (Vanderweyde et al., 2016).

The age-dependent aggregation of sgRBPs and prevalence of stress granule components in neurodegenerative diseases underline their relevance as therapeutic targets. One successful strategy would be to prevent the initial assembly of stress granules (Kim et al., 2014). Our work suggests another possibility,

Figure 5. HSF-1 Activity during Development Protects against PAB-1 Aggregation in Adulthood in *daf-2* Mutant and Wild-Type Adults

(A) Delayed tagRFP::PAB-1 aggregation with age in *daf-2* mutant background. Days 5 and 7, *daf-2(–)* versus wild-type background: ****p < 0.0001.

(B) Delayed Venus::TIAR-2 aggregation with age in *daf-2* mutant background. Days 1, 4 and 7, *daf-2(–)* versus wild-type background: *p < 0.05, **p < 0.01, and ****p < 0.0001, respectively.

(C) Levels of tagRFP::PAB-1 aggregation are highly increased at all ages examined in *hsf-1(–); daf-2(–)* animals compared with *daf-2(–)* animals. DAF-16 moderately protects against tagRFP::PAB-1 aggregation at day 11. *daf-2(–)* compared with *hsf-1(–);daf-2(–)*: ****p < 0.0001; *daf-2(–)* compared with *daf-16(–);daf-2(–)*: *p = 0.02.

(D) Head regions of representative animals expressing *Pmyo-2::tagRFP::PAB-1* in *daf-2(–), hsf-1(–); daf-2 (–)* and *daf-16(–); daf-2(–)* mutants at day 11. Scale bars: z stack projection, 15 μm; single-plane zoom, 5 μm.

(E) *hsf-1* mutation alone increases tagRFP::PAB-1 aggregation dramatically, even at day 2. ****p < 0.0001.

(F) HSF-1 activity during development is essential in order to delay tagRFP::PAB-1 aggregation (control: L4440 empty vector). Days 1 and 2 with RNAi treatment from egg, ****p < 0.0001.

(G) Delayed KIN-19::mEOS (monomeric EOS) aggregation with age in *daf-2* mutants is dependent on DAF-16, but not on HSF-1. *daf-2(–)* compared with *hsf-1(–); daf-2(–)*: day 2, **p = 0.0049; day 6, *p = 0.01. *daf-2(–)* compared with *daf-16(–);daf-2(–)*: ***p = 0.0003, day 10.

See also Figure S6 and Table S6.

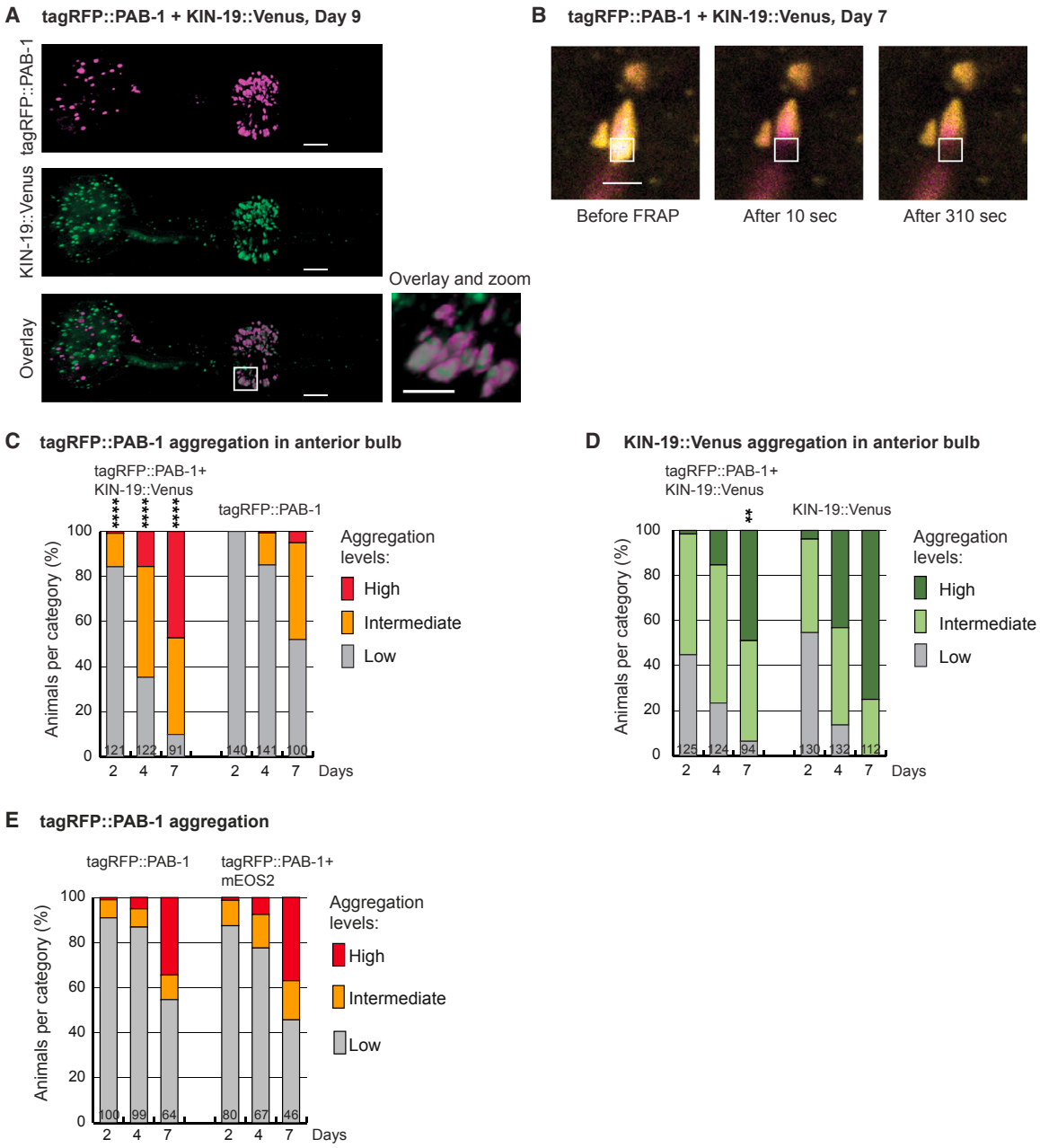

Figure 6. PAB-1 Aggregation Is Accelerated by KIN-19

(A) tagRFP::PAB-1 co-localizes with KIN-19::Venus in large aggregates in double-transgenic animals. Representative head region displayed in 3D. Scale bars, 10 μm; overlay and zoom scale bar, 5 μm.

(B) Representative immobile mixed tagRFP::PAB-1 (magenta) and KIN-19::Venus (yellow) puncta at day 7 assayed by FRAP. Bleached area is marked by white box. Scale bar, 2 μm.

(C) Accelerated tagRFP::PAB-1 aggregation in the anterior pharyngeal bulb in double transgenics compared with single transgenics. Days 2, 4, and 7: ****$p < 0.0001$.

(D) Moderately reduced KIN-19::Venus aggregation in the anterior pharyngeal bulb in double transgenics compared with single transgenics. Day 7: **$p = 0.0083$.

(E) No significant increase of tagRFP::PAB-1 aggregation in the presence of mEOS2 overexpression. At all ages, $p > 0.05$.

See also Figure S6.

namely abrogating sgRBP aggregation. In future work, it will be important to understand how longevity pathways relying on dietary restriction or defective mitochondrial respiration efficiently prevent sgRBP aggregation. In the case of reduced *daf-2* signaling, sgRBP aggregation is suppressed by at least two mechanisms: DAF-16 activation prevents cross-seeding by

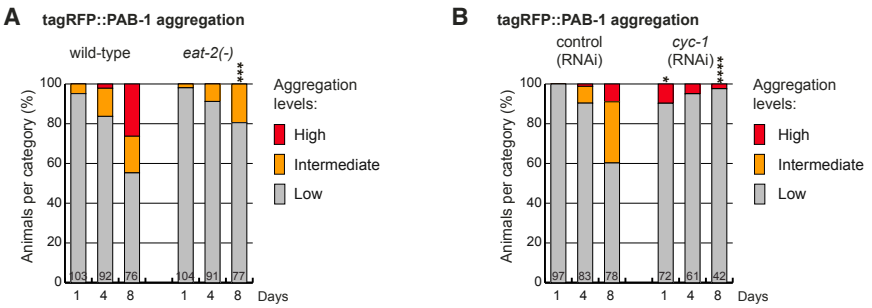

Figure 7. Other Longevity Pathways Prevent PAB-1 Aggregation with Age

(A) Dietary restriction delays tagRFP::PAB-1 aggregation with age. Day 8, *eat-2(–)* versus wild-type background: ***p < 0.001.

(B) Inhibition of mitochondrial function by *cyc-1* RNAi halts tagRFP::PAB-1 aggregation. Days 1 and 8, *cyc-1* RNAi versus control: *p < 0.05 and ****p < 0.0001, respectively.

delaying the accumulation of misfolded aggregation-prone proteins, and increased activity of HSF-1 during development assures enhanced sgRBP proteostasis throughout adulthood. To date, cross-seeding of RBP aggregation has been observed only with the Huntingtin protein containing an expanded polyglutamine repeat region (Furukawa et al., 2009). It will be important to investigate by which means endogenous aggregation-prone proteins lacking motifs similar to the LC prion-like domain would cross-seed RBPs aggregation. Overall, both of these strategies used to restore the dynamic nature of stress granule proteins could also directly prevent disease-associated RBP aggregation.

EXPERIMENTAL PROCEDURES

A list of strains, strain maintenance, RNAi treatment, and lifespan assays is described in the Supplemental Experimental Procedures.

Heat Shock

Nematodes were heat shocked in M9 medium with OP50 on a nutator. Control worms were treated the same at 20°C. Worms were either fixed for imaging analysis directly after heat shock or allowed to recover on normal growth (NG) plates kept at 20°C before fixation.

Size Measurements

Images were taken of synchronized live *C. elegans* using a Leica fluorescence microscope M165 FC with a Planapo 2.0× objective and Leica DFC310 FX camera. Body length was determined for each worm using Fiji software (Schindelin et al., 2012). Significance was evaluated by unpaired, two-tailed t test using GraphPad Prism 6.

Imaging and Immunofluorescence Staining

Worms were examined with a Leica SP8 confocal microscope. Fixation and immunostaining protocol including imaging parameters are described in the Supplemental Experimental Procedures. Representative confocal images are displayed as maximum z stack projection unless mentioned otherwise.

Aggregation Quantification In Vivo

In a population of synchronized live *C. elegans*, aggregation levels were determined using a Leica fluorescence microscope M165 FC with a Planapo 2.0× objective. Animals overexpressing *Pmyo-2::Venus::TIAR-2* were divided into two categories: animals with up to 10 (low aggregation) or more than 10 Venus::TIAR-2 puncta (intermediate aggregation) in the anterior and posterior pharyngeal bulb. Animals overexpressing *Pmyo-2:tagRFP:PAB-1* were divided into three categories: animals with up to 10 (low aggregation) or more than 10 (intermediate aggregation) tagRFP::PAB-1 puncta in the posterior bulb, or more than 10 (high aggregation) tagRFP:PAB-1 puncta in the anterior bulb. The latter mostly had more than 10 puncta in the posterior bulb. Animals expressing *Pkin-19::KIN-19::mEOS* or *Pkin-19::KIN-19::Venus* were divided into less than 10 puncta (low aggregation), between 10 and 100 puncta (intermediate aggregation), and more than 100 puncta in the anterior bulb (high aggregation). To compare aggregation levels between KIN-19::Venus and tagRFP::PAB-1, we evaluated tagRFP::PAB-1 puncta formation only in the anterior bulb and with the same counting scheme as for KIN-19::Venus. When comparing different strains, counting was done in a blind fashion. For statistics, two-tailed Fisher's exact test was performed using an online tool (http://www.socscistatistics.com/tests/fisher/default2.aspx). Significance of high + intermediate against low aggregation levels was calculated unless indicated otherwise. Numbers of animals per time point are indicated in the graphic bars.

FRAP Analysis

FRAP analysis was performed as previously described (David et al., 2010) using the Leica SP8 confocal microscope with the harmonic compound, plan, apochromatic (HC PL APO) CS2 63× 1.30 glycerol objective and photomultiplier tube (PMT) detector. Further experimental details are described in the Supplemental Experimental Procedures.

Insoluble Protein Extraction, Quantification, and Mass Spectrometry Analysis

To obtain large synchronized populations of aged animals and quantify protein aggregation only in the somatic tissues, we used temperature-induced sterile *gon-2* mutants as previously described (David et al., 2010). To induce longevity, we subjected animals to *daf-2* RNAi and control animals to *gfp* RNAi from the last larval stage L4 onward. Animals aged at 25°C were collected at day 3 of adulthood (young) and when half the control animals had died between days 14 and 18 (aged). No significant death was observed in long-lived animals on *daf-2* RNAi. Isolation of large SDS insoluble aggregates for immunoblot and mass spectrometry analysis were performed as previously described (David et al., 2010). See Supplemental Experimental Procedures for further details and antibodies used for immunoblots. The mass spectrometry proteomics data have been deposited to the ProteomeXchange Consortium (http://proteomecentral.proteomexchange.org) via the PRIDE partner repository (Vizcaíno et al., 2014) with the dataset identifier PXD003451.

Bioinformatics Analysis

Aliphatic amino acid residues were defined as A, G, I, L, and V. Secondary structure content was predicted using PSIPRED v2.6 (Jones, 1999). The p values were calculated using the unequal variance t test compared with the background set of all proteins detected by mass spectrometry (n = 5,637). Additional details and functional analysis are described in the Supplemental Experimental Procedures.

ACCESSION NUMBERS

The accession number for the mass spectrometry proteomics data reported in this paper is PRIDE: PXD003451.

SUPPLEMENTAL INFORMATION

Supplemental Information includes Supplemental Experimental Procedures, six figures, six tables, and one movie and can be found with this article online at http://dx.doi.org/10.1016/j.celrep.2016.12.033.

AUTHOR CONTRIBUTIONS

M.C.L., N.G., J.C.T., and D.C.D. designed and performed experiments. E.D.C. performed bioinformatics analysis. K.W., R.J., and J.K. generated reagents. J.K. performed chaperone immunostainings. A.L.B. provided analytical tools, reagents, and materials. M.C.L., J.C.T., and D.C.D. wrote the paper.

ACKNOWLEDGMENTS

We are grateful to Cynthia Kenyon for help in the early stages of this project. We thank Aimee Kao and Sivan Henis-Korenblit for critical input, David Maltby for mass spectrometry support, Aenoch Lynn for help with the proteomic data analysis, Brian Lee for basic gateway constructs, and Kristin Arnsburg for integrating DNJ-13 and DNJ-19 transgenics. We are grateful to Simon Alberti for sharing the *C. elegans* list of proteins with prion-like domains. For the generous donation of antibodies, we would like to thank Rafal Ciosk (anti-PAB-1), Junho Lee (anti-HRP-1), and Keith Blackwell (anti-CAR-1). The *gon-2* mutants were kindly provided by Eric Lambie. This work was initiated in Cynthia Kenyon's lab and was funded by an Ellison/AFAR postdoctoral fellowship (to D.C.D.) and by the NIH (NIGMS grant 8P41GM103481 to A.L.B. and grant P50 GM081879 to J.C.T. and A.L.B.). Subsequently, this work was supported by funding from the DZNE and a Marie Curie International Reintegration Grant (322120 to D.C.D.).

Received: August 11, 2016
Revised: October 28, 2016
Accepted: December 12, 2016
Published: January 10, 2017

REFERENCES

Alberti, S., Halfmann, R., King, O., Kapila, A., and Lindquist, S. (2009). A systematic survey identifies prions and illuminates sequence features of prionogenic proteins. Cell *137*, 146–158.

Arai, T., Hasegawa, M., Akiyama, H., Ikeda, K., Nonaka, T., Mori, H., Mann, D., Tsuchiya, K., Yoshida, M., Hashizume, Y., and Oda, T. (2006). TDP-43 is a component of ubiquitin-positive tau-negative inclusions in frontotemporal lobar degeneration and amyotrophic lateral sclerosis. Biochem. Biophys. Res. Commun. *351*, 602–611.

Aulas, A., and Vande Velde, C. (2015). Alterations in stress granule dynamics driven by TDP-43 and FUS: a link to pathological inclusions in ALS? Front. Cell. Neurosci. *9*, 423.

Ayyadevara, S., Mercanti, F., Wang, X., Mackintosh, S.G., Tackett, A.J., Prayaga, S.V., Romeo, F., Shmookler Reis, R.J., and Mehta, J.L. (2016). Age- and hypertension-associated protein aggregates in mouse heart have similar proteomic profiles. Hypertension *67*, 1006–1013.

Balch, W.E., Morimoto, R.I., Dillin, A., and Kelly, J.W. (2008). Adapting proteostasis for disease intervention. Science *319*, 916–919.

Bentmann, E., Neumann, M., Tahirovic, S., Rodde, R., Dormann, D., and Haass, C. (2012). Requirements for stress granule recruitment of fused in sarcoma (FUS) and TAR DNA-binding protein of 43 kDa (TDP-43). J. Biol. Chem. *287*, 23079–23094.

Bentmann, E., Haass, C., and Dormann, D. (2013). Stress granules in neurodegeneration–lessons learnt from TAR DNA binding protein of 43 kDa and fused in sarcoma. FEBS J. *280*, 4348–4370.

Brais, B., Bouchard, J.P., Xie, Y.G., Rochefort, D.L., Chrétien, N., Tomé, F.M., Lafrenière, R.G., Rommens, J.M., Uyama, E., Nohira, O., et al. (1998). Short GCG expansions in the PABP2 gene cause oculopharyngeal muscular dystrophy. Nat. Genet. *18*, 164–167.

Cherkasov, V., Hofmann, S., Druffel-Augustin, S., Mogk, A., Tyedmers, J., Stoecklin, G., and Bukau, B. (2013). Coordination of translational control and protein homeostasis during severe heat stress. Curr. Biol. *23*, 2452–2462.

David, D.C. (2012). Aging and the aggregating proteome. Front. Genet. *3*, 247.

David, D.C., Ollikainen, N., Trinidad, J.C., Cary, M.P., Burlingame, A.L., and Kenyon, C. (2010). Widespread protein aggregation as an inherent part of aging in C. elegans. PLoS Biol. *8*, e1000450.

Demontis, F., and Perrimon, N. (2010). FOXO/4E-BP signaling in Drosophila muscles regulates organism-wide proteostasis during aging. Cell *143*, 813–825.

Eulalio, A., Behm-Ansmant, I., and Izaurralde, E. (2007). P bodies: at the crossroads of post-transcriptional pathways. Nat. Rev. Mol. Cell Biol. *8*, 9–22.

Furukawa, Y., Kaneko, K., Matsumoto, G., Kurosawa, M., and Nukina, N. (2009). Cross-seeding fibrillation of Q/N-rich proteins offers new pathomechanism of polyglutamine diseases. J. Neurosci. *29*, 5153–5162.

Gilks, N., Kedersha, N., Ayodele, M., Shen, L., Stoecklin, G., Dember, L.M., and Anderson, P. (2004). Stress granule assembly is mediated by prion-like aggregation of TIA-1. Mol. Biol. Cell *15*, 5383–5398.

Goudeau, J., and Aguilaniu, H. (2010). Carbonylated proteins are eliminated during reproduction in C. elegans. Aging Cell *9*, 991–1003.

Han, T.W., Kato, M., Xie, S., Wu, L.C., Mirzaei, H., Pei, J., Chen, M., Xie, Y., Allen, J., Xiao, G., and McKnight, S.L. (2012). Cell-free formation of RNA granules: bound RNAs identify features and components of cellular assemblies. Cell *149*, 768–779.

Hsu, A.L., Murphy, C.T., and Kenyon, C. (2003). Regulation of aging and age-related disease by DAF-16 and heat-shock factor. Science *300*, 1142–1145.

Johnson, B.S., Snead, D., Lee, J.J., McCaffery, J.M., Shorter, J., and Gitler, A.D. (2009). TDP-43 is intrinsically aggregation-prone, and amyotrophic lateral sclerosis-linked mutations accelerate aggregation and increase toxicity. J. Biol. Chem. *284*, 20329–20339.

Jones, D.T. (1999). Protein secondary structure prediction based on position-specific scoring matrices. J. Mol. Biol. *292*, 195–202.

Kato, M., Han, T.W., Xie, S., Shi, K., Du, X., Wu, L.C., Mirzaei, H., Goldsmith, E.J., Longgood, J., Pei, J., et al. (2012). Cell-free formation of RNA granules: low complexity sequence domains form dynamic fibers within hydrogels. Cell *149*, 753–767.

Kenyon, C.J. (2010). The genetics of ageing. Nature *464*, 504–512.

Kim, H.J., Kim, N.C., Wang, Y.D., Scarborough, E.A., Moore, J., Diaz, Z., MacLea, K.S., Freibaum, B., Li, S., Molliex, A., et al. (2013). Mutations in prion-like domains in hnRNPA2B1 and hnRNPA1 cause multisystem proteinopathy and ALS. Nature *495*, 467–473.

Kim, H.J., Raphael, A.R., LaDow, E.S., McGurk, L., Weber, R.A., Trojanowski, J.Q., Lee, V.M., Finkbeiner, S., Gitler, A.D., and Bonini, N.M. (2014). Therapeutic modulation of eIF2α phosphorylation rescues TDP-43 toxicity in amyotrophic lateral sclerosis disease models. Nat. Genet. *46*, 152–160.

King, O.D., Gitler, A.D., and Shorter, J. (2012). The tip of the iceberg: RNA-binding proteins with prion-like domains in neurodegenerative disease. Brain Res. *1462*, 61–80.

Klar, J., Sobol, M., Melberg, A., Mäbert, K., Ameur, A., Johansson, A.C., Feuk, L., Entesarian, M., Orlén, H., Casar-Borota, O., and Dahl, N. (2013). Welander distal myopathy caused by an ancient founder mutation in TIA1 associated with perturbed splicing. Hum. Mutat. *34*, 572–577.

Kroschwald, S., Maharana, S., Mateju, D., Malinovska, L., Nüske, E., Poser, I., Richter, D., and Alberti, S. (2015). Promiscuous interactions and protein disaggregases determine the material state of stress-inducible RNP granules. eLife *4*, e06807.

Li, Y.R., King, O.D., Shorter, J., and Gitler, A.D. (2013). Stress granules as crucibles of ALS pathogenesis. J. Cell Biol. *201*, 361–372.

Lin, K., Dorman, J.B., Rodan, A., and Kenyon, C. (1997). daf-16: an HNF-3/forkhead family member that can function to double the life-span of Caenorhabditis elegans. Science *278*, 1319–1322.

Lin, Y., Protter, D.S., Rosen, M.K., and Parker, R. (2015). Formation and maturation of phase-separated liquid droplets by RNA-binding proteins. Mol. Cell *60*, 208–219.

Molliex, A., Temirov, J., Lee, J., Coughlin, M., Kanagaraj, A.P., Kim, H.J., Mittag, T., and Taylor, J.P. (2015). Phase separation by low complexity domains

promotes stress granule assembly and drives pathological fibrillization. Cell *163*, 123–133.

Mori, K., Lammich, S., Mackenzie, I.R., Forné, I., Zilow, S., Kretzschmar, H., Edbauer, D., Janssens, J., Kleinberger, G., Cruts, M., et al. (2013). hnRNP A3 binds to GGGGCC repeats and is a constituent of p62-positive/TDP43-negative inclusions in the hippocampus of patients with C9orf72 mutations. Acta Neuropathol. *125*, 413–423.

Murakami, T., Yang, S.P., Xie, L., Kawano, T., Fu, D., Mukai, A., Bohm, C., Chen, F., Robertson, J., Suzuki, H., et al. (2012). ALS mutations in FUS cause neuronal dysfunction and death in Caenorhabditis elegans by a dominant gain-of-function mechanism. Hum. Mol. Genet. *21*, 1–9.

Murakami, T., Qamar, S., Lin, J.Q., Schierle, G.S., Rees, E., Miyashita, A., Costa, A.R., Dodd, R.B., Chan, F.T., Michel, C.H., et al. (2015). ALS/FTD mutation-induced phase transition of FUS liquid droplets and reversible hydrogels into irreversible hydrogels impairs RNP granule function. Neuron *88*, 678–690.

Neumann, M., Sampathu, D.M., Kwong, L.K., Truax, A.C., Micsenyi, M.C., Chou, T.T., Bruce, J., Schuck, T., Grossman, M., Clark, C.M., et al. (2006). Ubiquitinated TDP-43 in frontotemporal lobar degeneration and amyotrophic lateral sclerosis. Science *314*, 130–133.

Neumann, M., Rademakers, R., Roeber, S., Baker, M., Kretzschmar, H.A., and Mackenzie, I.R. (2009). A new subtype of frontotemporal lobar degeneration with FUS pathology. Brain *132*, 2922–2931.

Neumann, M., Bentmann, E., Dormann, D., Jawaid, A., DeJesus-Hernandez, M., Ansorge, O., Roeber, S., Kretzschmar, H.A., Munoz, D.G., Kusaka, H., et al. (2011). FET proteins TAF15 and EWS are selective markers that distinguish FTLD with FUS pathology from amyotrophic lateral sclerosis with FUS mutations. Brain *134*, 2595–2609.

Ogg, S., Paradis, S., Gottlieb, S., Patterson, G.I., Lee, L., Tissenbaum, H.A., and Ruvkun, G. (1997). The Fork head transcription factor DAF-16 transduces insulin-like metabolic and longevity signals in C. elegans. Nature *389*, 994–999.

Patel, A., Lee, H.O., Jawerth, L., Maharana, S., Jahnel, M., Hein, M.Y., Stoynov, S., Mahamid, J., Saha, S., Franzmann, T.M., et al. (2015). A liquid-to-solid phase transition of the ALS protein FUS accelerated by disease mutation. Cell *162*, 1066–1077.

Reis-Rodrigues, P., Czerwieniec, G., Peters, T.W., Evani, U.S., Alavez, S., Gaman, E.A., Vantipalli, M., Mooney, S.D., Gibson, B.W., Lithgow, G.J., and Hughes, R.E. (2012). Proteomic analysis of age-dependent changes in protein solubility identifies genes that modulate lifespan. Aging Cell *11*, 120–127.

Rousakis, A., Vlanti, A., Borbolis, F., Roumelioti, F., Kapetanou, M., and Syntichaki, P. (2014). Diverse functions of mRNA metabolism factors in stress defense and aging of Caenorhabditis elegans. PLoS ONE *9*, e103365.

Schindelin, J., Arganda-Carreras, I., Frise, E., Kaynig, V., Longair, M., Pietzsch, T., Preibisch, S., Rueden, C., Saalfeld, S., Schmid, B., et al. (2012). Fiji: an open-source platform for biological-image analysis. Nat. Methods *9*, 676–682.

Tanase, M., Urbanska, A.M., Zolla, V., Clement, C.C., Huang, L., Morozova, K., Follo, C., Goldberg, M., Roda, B., Reschiglian, P., and Santambrogio, L. (2016). Role of carbonyl modifications on aging-associated protein aggregation. Sci. Rep. *6*, 19311.

Taylor, R.C., and Dillin, A. (2011). Aging as an event of proteostasis collapse. Cold Spring Harb. Perspect. Biol. *3*, a004440.

Tollervey, D., Lehtonen, H., Carmo-Fonseca, M., and Hurt, E.C. (1991). The small nucleolar RNP protein NOP1 (fibrillarin) is required for pre-rRNA processing in yeast. EMBO J. *10*, 573–583.

Vanderweyde, T., Apicco, D.J., Youmans-Kidder, K., Ash, P.E., Cook, C., Lummertz da Rocha, E., Jansen-West, K., Frame, A.A., Citro, A., Leszyk, J.D., et al. (2016). Interaction of tau with the RNA-binding protein TIA1 regulates tau pathophysiology and toxicity. Cell Rep. *15*, 1455–1466.

Vizcaíno, J.A., Deutsch, E.W., Wang, R., Csordas, A., Reisinger, F., Ríos, D., Dianes, J.A., Sun, Z., Farrah, T., Bandeira, N., et al. (2014). ProteomeXchange provides globally coordinated proteomics data submission and dissemination. Nat. Biotechnol. *32*, 223–226.

Volovik, Y., Maman, M., Dubnikov, T., Bejerano-Sagie, M., Joyce, D., Kapernick, E.A., Cohen, E., and Dillin, A. (2012). Temporal requirements of heat shock factor-1 for longevity assurance. Aging Cell *11*, 491–499.

Walters, R.W., Muhlrad, D., Garcia, J., and Parker, R. (2015). Differential effects of Ydj1 and Sis1 on Hsp70-mediated clearance of stress granules in Saccharomyces cerevisiae. RNA *21*, 1660–1671.

Walther, D.M., Kasturi, P., Zheng, M., Pinkert, S., Vecchi, G., Ciryam, P., Morimoto, R.I., Dobson, C.M., Vendruscolo, M., Mann, M., and Hartl, F.U. (2015). Widespread proteome remodeling and aggregation in aging C. elegans. Cell *161*, 919–932.

Zimmerman, S.M., Hinkson, I.V., Elias, J.E., and Kim, S.K. (2015). Reproductive aging drives protein accumulation in the uterus and limits lifespan in C. elegans. PLoS Genet. *11*, e1005725.

Cell Reports, Volume *18*

Supplemental Information

Reduced Insulin/IGF-1 Signaling Restores the Dynamic Properties of Key Stress Granule Proteins during Aging

Marie C. Lechler, Emily D. Crawford, Nicole Groh, Katja Widmaier, Raimund Jung, Janine Kirstein, Jonathan C. Trinidad, Alma L. Burlingame, and Della C. David

Figure S1

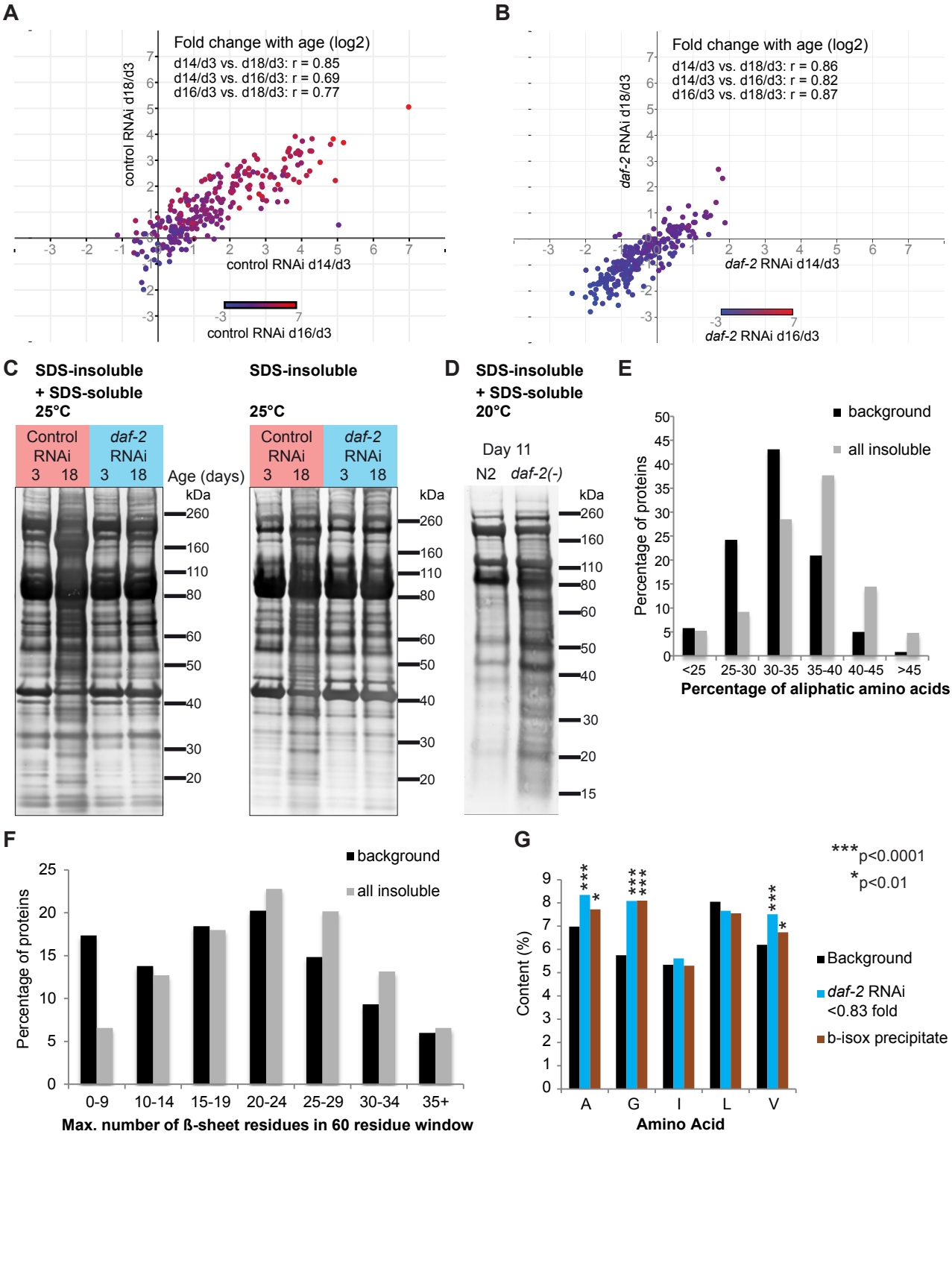
A
Fold change with age (log2)
d14/d3 vs. d18/d3: r = 0.85
d14/d3 vs. d16/d3: r = 0.69
d16/d3 vs. d18/d3: r = 0.77
control RNAi d18/d3
control RNAi d14/d3
control RNAi d16/d3
B
Fold change with age (log2)
d14/d3 vs. d18/d3: r = 0.86
d14/d3 vs. d16/d3: r = 0.82
d16/d3 vs. d18/d3: r = 0.87
daf-2 RNAi d18/d3
daf-2 RNAi d14/d3
daf-2 RNAi d16/d3
C
SDS-insoluble
+ SDS-soluble
25°C
Control RNAi
daf-2 RNAi
3 18 3 18
Age (days)
kDa
260
160
110
80
60
50
40
30
20
SDS-insoluble
25°C
D
SDS-insoluble
+ SDS-soluble
20°C
Day 11
N2 daf-2(-)
E
background
all insoluble
Percentage of proteins
<25 25-30 30-35 35-40 40-45 >45
Percentage of aliphatic amino acids
F
background
all insoluble
Percentage of proteins
0-9 10-14 15-19 20-24 25-29 30-34 35+
Max. number of ß-sheet residues in 60 residue window
G
***p<0.0001
*p<0.01
Background
daf-2 RNAi
<0.83 fold
b-isox precipitate
Content (%)
A G I L V
Amino Acid

Figure S1. Changes in insolubility with age are highly correlated between the three biological replicates. Related to Figure 1.

(A) Fold changes in insolubility with age in animals treated with control RNAi are plotted for three biological replicates. Spearman r correlation r= 0.77 d18/d3 versus d16/d3, r= 0.85 d18/d3 versus d14/d3 and r= 0.67 d14/d3 versus d16/d3; two-tailed p-value p<0.0001 d18/d3 versus d16/d3, p<0.0001 d18/d3 versus d14/d3 and p<0.0001 d14/d3 versus d16/d3.

(B) Fold changes in insolubility with age in animals treated with *daf-2* RNAi are plotted for three biological replicates. Spearman r correlation r= 0.87 d18/d3 versus d16/d3, r= 0.86 d18/d3 versus d14/d3 and r= 0.82 d14/d3 versus d16/d3; two-tailed p-value p<0.0001 d18/d3 versus d16/d3, p<0.0001 d18/d3 versus d14/d3 and p<0.0001 d14/d3 versus d16/d3.

(C) Sypro Ruby whole protein staining of [SDS-soluble + SDS-insoluble] fraction and SDS-insoluble fraction from day 3 and day 18 *gon-2(-)* mutants exposed to control and *daf-2* RNAi (grown at 25°C).

(D) Sypro Ruby whole protein staining of [SDS-soluble + SDS-insoluble] fraction from aged (day 11) wildtype (N2) and *daf-2(-)* mutants (grown at 20°C).

(E) Aggregation-prone proteins (all insoluble proteins, n= 228) are enriched in aliphatic amino acids.
Unequal variance t-test: p= 3.7E-14.

(F) Aggregation-prone proteins (all insoluble proteins, n= 228) are enriched in extended stretches of β-sheet propensity. Unequal variance t-test: p= 7.9E-7.

(G) Alanine, glycine and valine are significantly enriched in aggregation-prone proteins selectively targeted by long-lived *daf-2(-)* animals compared to the background proteome (<0.83 fold change in aggregation in *daf-2(-)* conditions, n= 81, unequal variance t test: A, p= 9.6E-5, G, p= 1.1E-5, V, p= 1.3E-6). Similarly, these three amino acids are enriched in proteins precipitated by b-isox (n= 126, unequal variance t test: A, p= 0.007, G, p= 8.8E-9, V, p= 0.004).

Figure S2

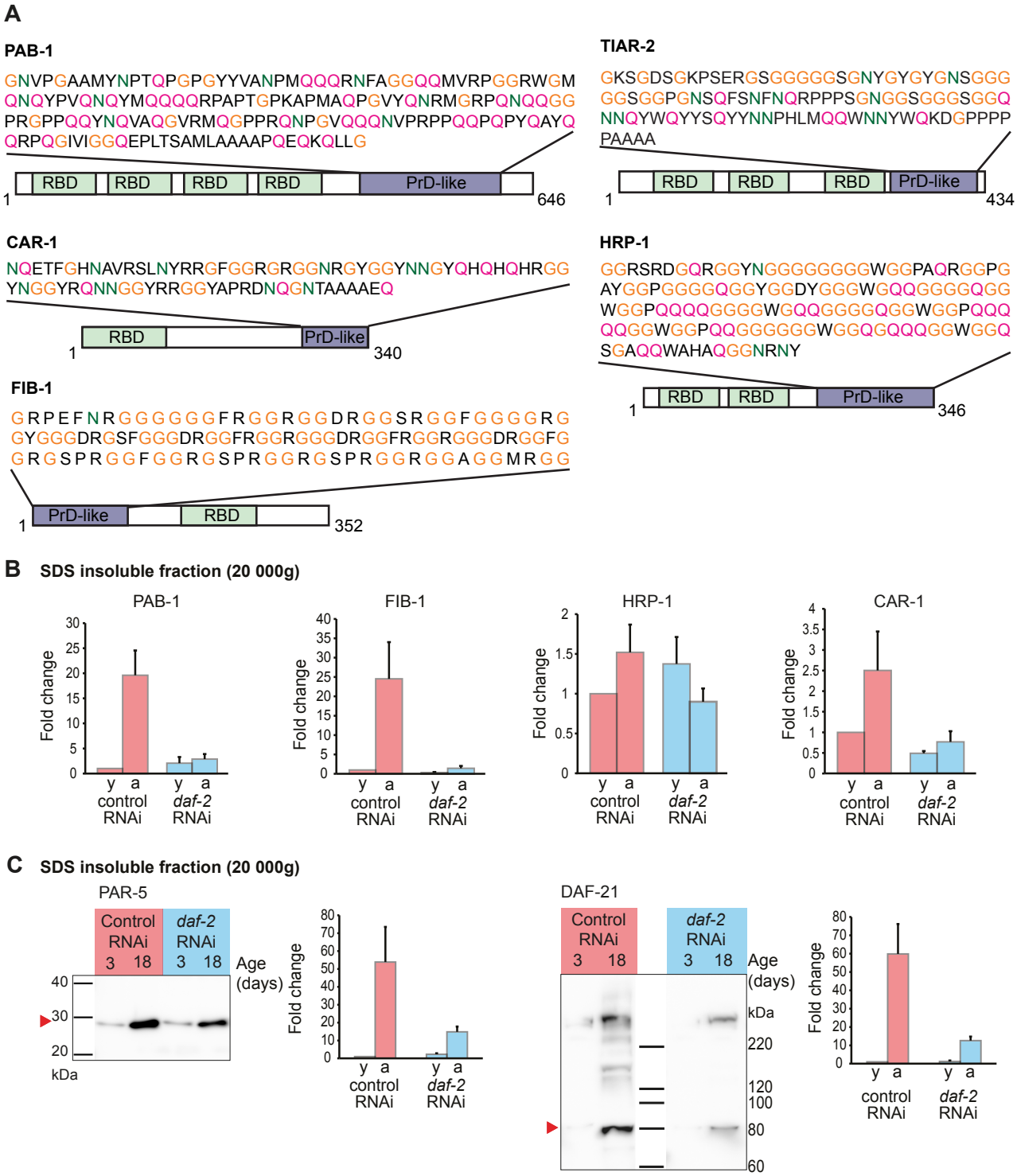

Figure S2: Reduced *daf-2* signaling efficiently prevents age-dependent insolubility of RBP with LC "prion-like" domains. Related to Figure 1.

(A) Graphical depiction of PAB-1, TIAR-2, HRP-1, CAR-1 and FIB-1. Green boxes represent RNA-binding domains (RBD) and purple boxes prion-like LC domains (PrD-like). Amino acid sequences of PrDs are detailed. Amino acids enriched in PrD-like domains: glycines, glutamines and asparagines are coloured.

(B) Quantifications of immunoblots detecting RBPs PAB-1, FIB-1, HRP-1 and CAR-1 in the SDS-insoluble fraction. The averages of three biological replicates ± SEM are represented.

(C) Relevant protein bands indicated by red arrow. Quantifications of immunoblots detecting PAR-5 and DAF-21 in the SDS-insoluble fraction. The averages of three biological replicates ± SEM are represented.

Figure S3

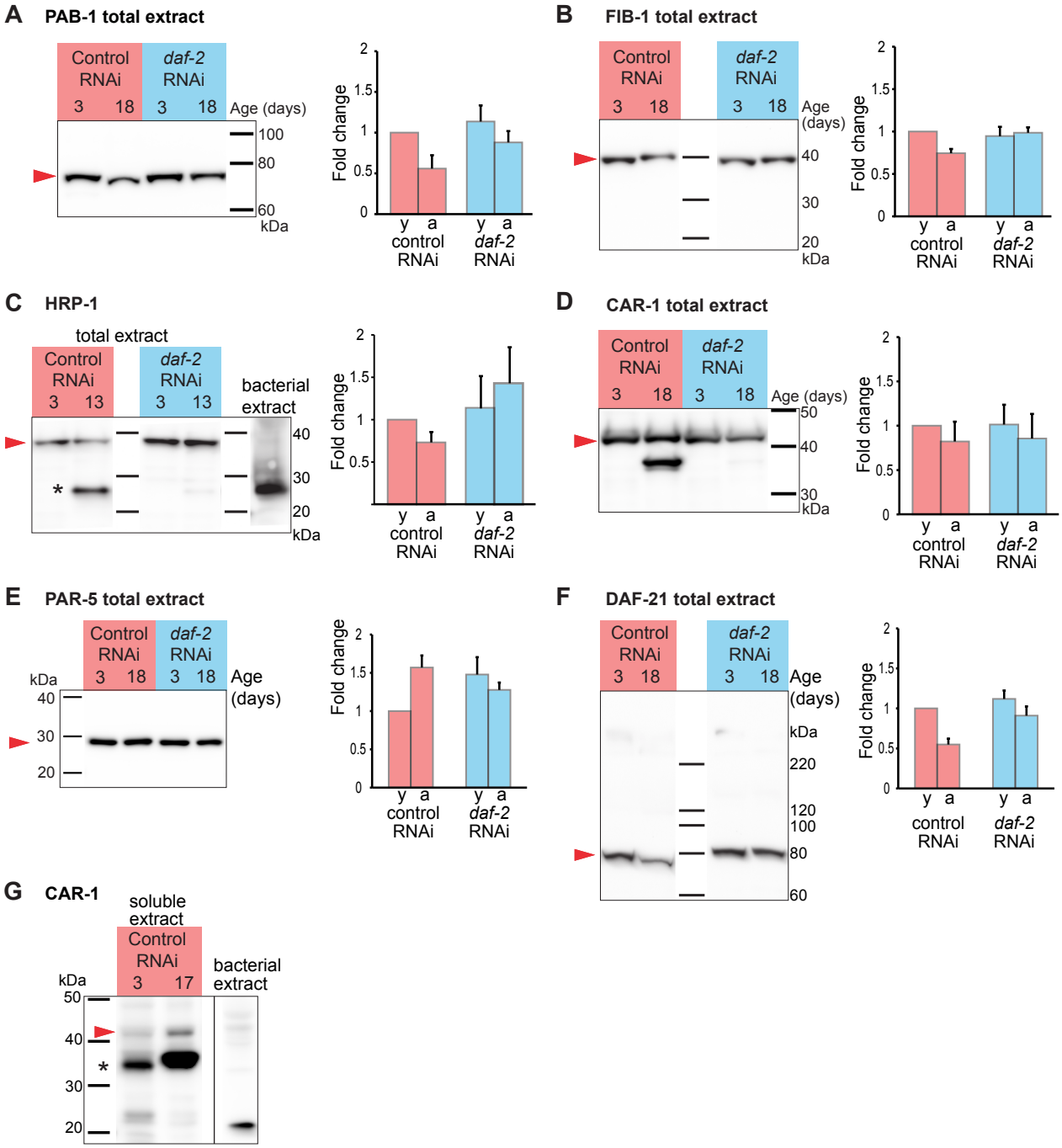

Figure S3. Total protein levels do not change upon *daf-2* inhibition. Related to Figure 1.
(A) Immunoblot of PAB-1 (red arrow) in the total extract.
(B) Immunoblot of FIB-1 (red arrow) in the total extract.
(C) Immunoblot of HRP-1 (red arrow) in the total extract. Truncated band between 20 and 30kDa (marked by asterisk) detected by anti-HRP-1 is due to cross-reaction with bacterial protein.
(D) Immunoblot of CAR-1 (red arrow) in the total extract.
(E) Immunoblot of PAR-5 (red arrow) in the total extract.
(F) Immunoblot of DAF-21 (red arrow) in the total extract.
(G) Truncated band between 30 and 40kDa (marked by asterisk) detected by anti-CAR-1 is not present in bacterial sample.
Quantifications represent the average of three biological replicates ± SEM. For the quantifications, total band levels were normalized to total protein levels detected by Sypro Ruby.

Figure S4

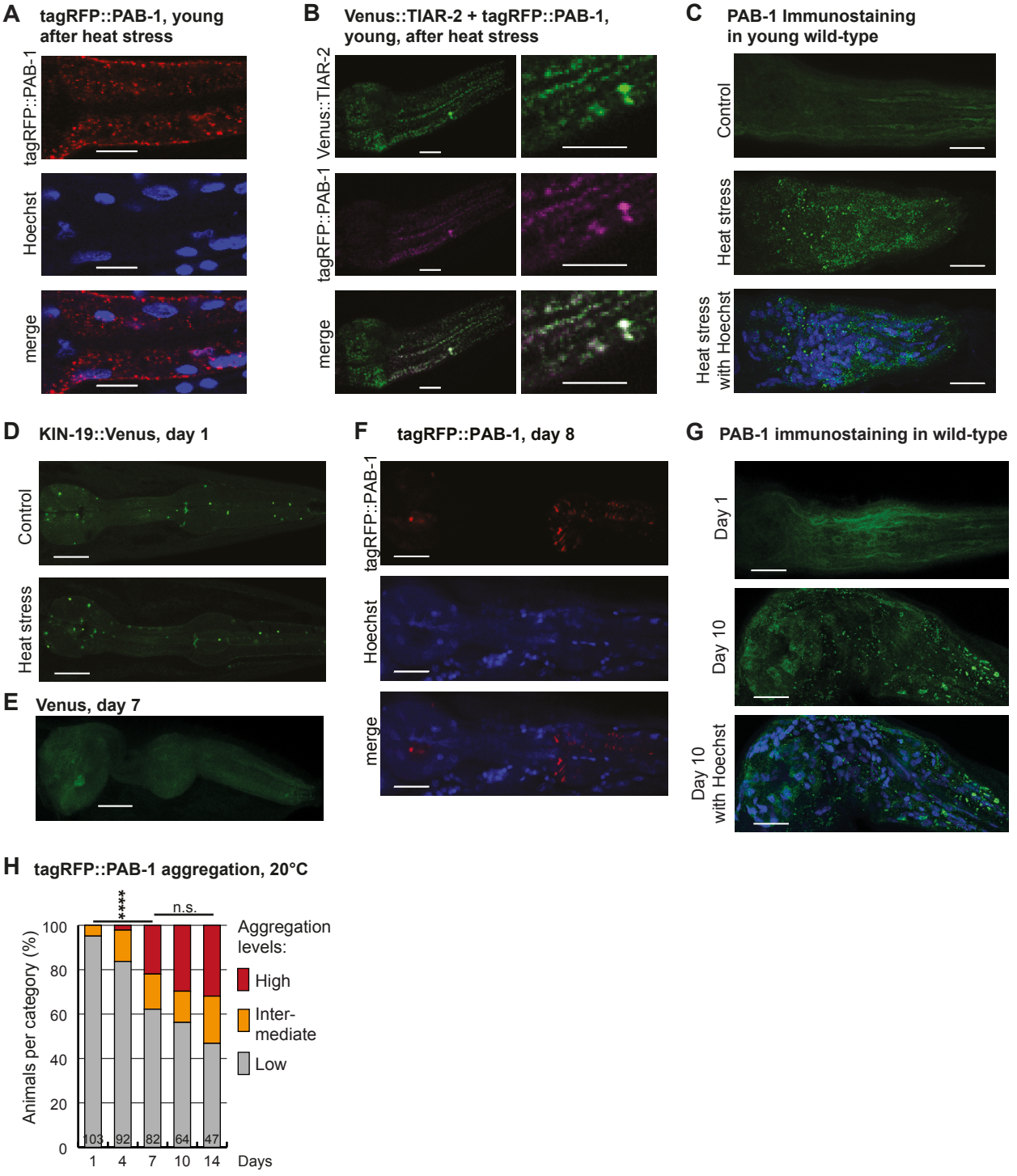
A
tagRFP::PAB-1, young after heat stress
tagRFP::PAB-1
Hoechst
merge
B
Venus::TIAR-2 + tagRFP::PAB-1, young, after heat stress
Venus::TIAR-2
tagRFP::PAB-1
merge
C
PAB-1 Immunostaining in young wild-type
Control
Heat stress
Heat stress with Hoechst
D
KIN-19::Venus, day 1
Control
Heat stress
E
Venus, day 7
F
tagRFP::PAB-1, day 8
tagRFP::PAB-1
Hoechst
merge
G
PAB-1 immunostaining in wild-type
Day 1
Day 10
Day 10 with Hoechst
H
tagRFP::PAB-1 aggregation, 20°C
****
n.s.
Animals per category (%)
100
80
60
40
20
0
103
92
82
64
47
1
4
7
10
14
Days
Aggregation levels:
High
Inter-mediate
Low

Figure S4. PAB-1 accumulates in puncta with age in wildtype *C. elegans*. Related to Figure 2.

(A) Zoom into the procorpus of tagRFP::PAB-1 expressed in the pharyngeal muscles showing cytoplasmic and nuclear tagRFP::PAB-1 stress granules upon heat stress (2h, 32°C) at day 1 of adulthood. Representative single plane confocal images. Scale bar 7µm.

(B) tagRFP::PAB-1 and Venus::TIAR-2 co-localize in stress granules upon heat stress (2h, 32°C). Experiment performed at day 2 of adulthood. Scale bar 7µm.

(C) Exposure to 35°C for 3h in wildtype N2 animals at day 1 leads to stress granule formation detected by PAB-1 antibody. Scale bar 15µm.

(D) KIN-19::Venus does not form stress granules after exposure to heat stress (32°C, 2h) as seen in the pharynx of worms expressing *Pkin-19::KIN-19::Venus* at day 1. Scale bar 15µm.

(E) Venus-tag alone does not aggregate with age in animals expressing *Pmyo2::Venus*, day 7. Scale bar 15µm.

(F) Animals expressing *Pmyo-2::tagRFP::PAB-1* at day 8 show cytoplasmic tagRFP::PAB-1 puncta. Representative single plane confocal images. Scale bar 15µm.

(G) Immunostaining of PAB-1 in the head region of wildtype N2 worms reveals a diffuse PAB-1 pattern at day 1 which changes into a punctate pattern at day 10. Scale bar 15µm.

(H) After day 7 of adulthood the increase in tagRFP::PAB-1 aggregation with age in *Pmyo-2::tagRFP::PAB-1* transgenics is not significant. Day 1 versus day 7: ****p<0.0001, day 7 versus day 14: n.s.=0.0999.

Figure S5

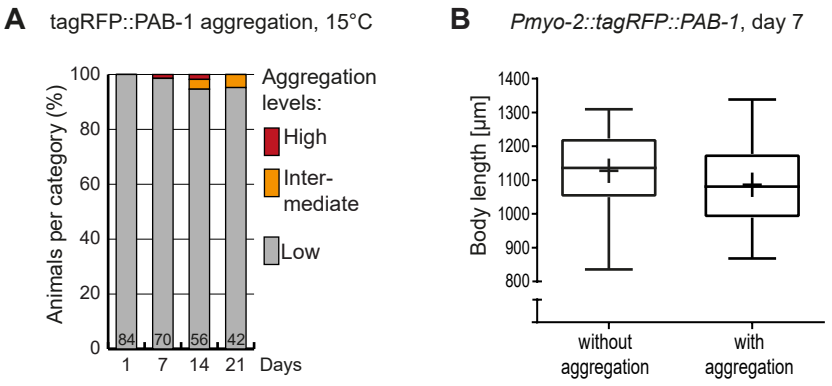

Figure S5. Age-dependent PAB-1 aggregation is associated with reduced body size. Related to Figure 4.
(A) No significant increase of tagRFP::PAB-1 aggregation in *Pmyo-2::tagRFP::PAB-1* transgenics grown at 15°C. At all ages $p>0.05$.
(B) Animals with tagRFP::PAB-1 aggregation are significantly smaller than animals without aggregation (biological repeat, day 7, $p=0.0041$). Data represented with Tukey-style box plots and mean indicated by + (animals without aggregation N = 100, with aggregation N = 149).

Figure S6

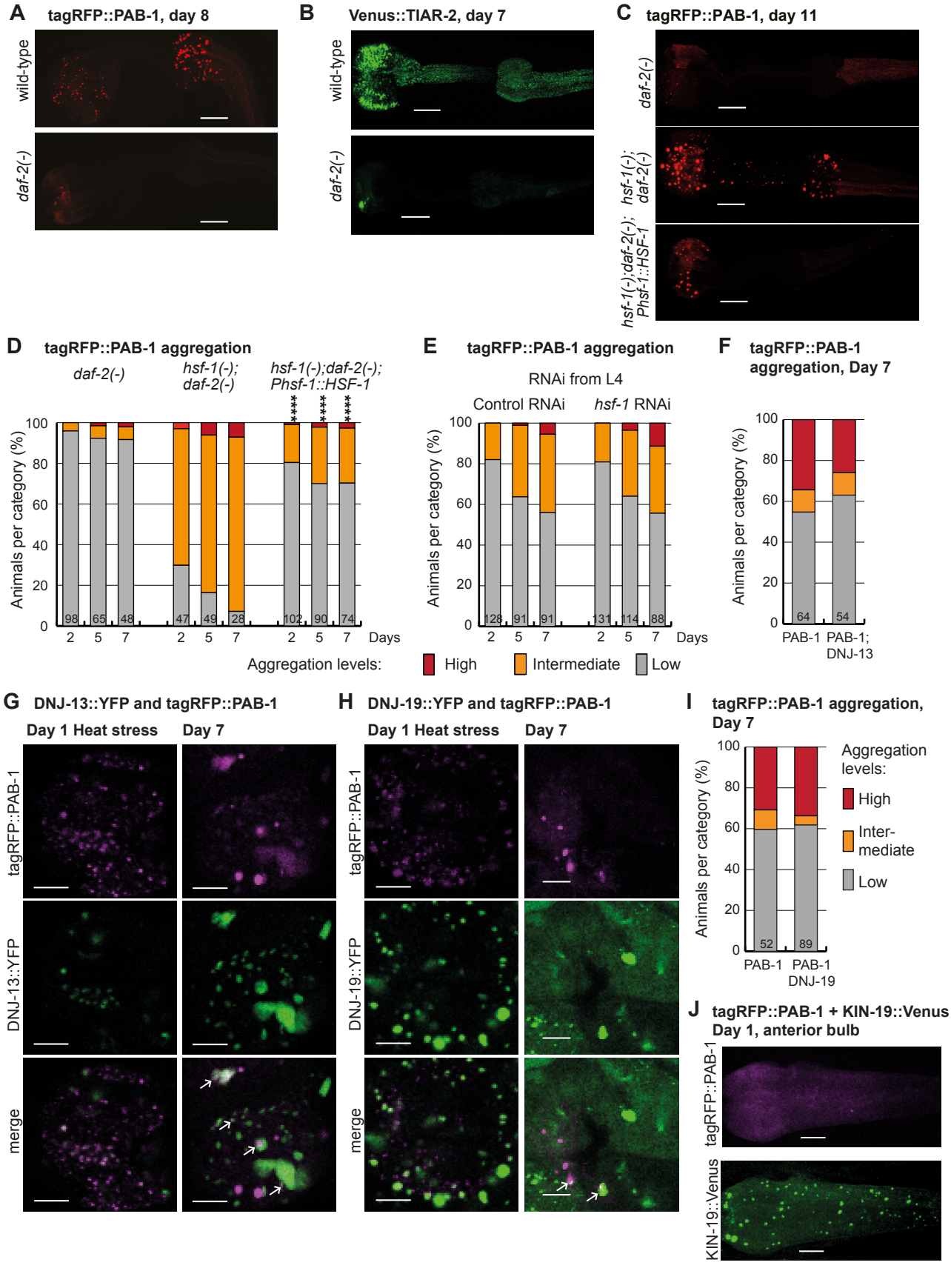
A
tagRFP::PAB-1, day 8
wild-type
daf-2(-)
B
Venus::TIAR-2, day 7
wild-type
daf-2(-)
C
tagRFP::PAB-1, day 11
daf-2(-)
hsf-1(-); daf-2(-)
hsf-1(-);daf-2(-); Phsf-1::HSF-1
D
tagRFP::PAB-1 aggregation
daf-2(-)
hsf-1(-); daf-2(-)
hsf-1(-);daf-2(-); Phsf-1::HSF-1
****
Animals per category (%)
100
80
60
40
20
0
98 65 48 47 49 28 102 90 74
2 5 7 2 5 7 2 5 7
Days
Aggregation levels:
High
Intermediate
Low
E
tagRFP::PAB-1 aggregation
RNAi from L4
Control RNAi
hsf-1 RNAi
Animals per category (%)
128 91 91 131 114 88
2 5 7 2 5 7
Days
F
tagRFP::PAB-1 aggregation, Day 7
Animals per category (%)
64 54
PAB-1
PAB-1; DNJ-13
G
DNJ-13::YFP and tagRFP::PAB-1
Day 1 Heat stress
Day 7
tagRFP::PAB-1
DNJ-13::YFP
merge
H
DNJ-19::YFP and tagRFP::PAB-1
Day 1 Heat stress
Day 7
tagRFP::PAB-1
DNJ-19::YFP
merge
I
tagRFP::PAB-1 aggregation, Day 7
Animals per category (%)
52 89
PAB-1
PAB-1 DNJ-19
Aggregation levels:
High
Inter-mediate
Low
J
tagRFP::PAB-1 + KIN-19::Venus
Day 1, anterior bulb
tagRFP::PAB-1
KIN-19::Venus

Figure S6. Colocalization of chaperones DNJ-13 and DNJ-19 with PAB-1 stress granules and age-dependent puncta does not influence PAB-1 aggregation levels. Related to Figure 5.
(A) *daf-2* mutants prevent tagRFP::PAB-1 puncta formation. Scale bar 15μm.
(B) *daf-2* mutants prevent Venus::TIAR-2 puncta formation. Scale bar 15μm.
(C) HSF-1 overexpression stops increased tagRFP::PAB-1 aggregation in day 11 *Pmyo-2::tagRFP::PAB-1* transgenics in the *hsf-1; daf-2* double mutant background. Scale bar 15μm.
(D) HSF-1 overexpression rescues effect of *hsf-1* mutation in *daf-2* mutant background. Day 2, day 5 and day 7, versus *hsf-1(-);daf-2(-)*,****p<0.0001.
(E) HSF-1 knockdown after development is not sufficient to delay tagRFP::PAB-1 aggregation. L4440 empty vector used as RNAi control. Fisher's exact test two-tailed not significant.
(F) No significant change in tagRFP::PAB-1 aggregation with age by DNJ-13::YFP overexpression in a population of *C. elegans* at day 7 (p>0.05).
(G) tagRFP::PAB-1 and DNJ-13::YFP colocalize in heat stress induced stress granules and age-related puncta. Arrows mark colocalization of chaperones with age-related puncta. Representative single plane images. Scale bar 5μm.
(H) tagRFP::PAB-1 and DNJ-19::YFP colocalize in heat stress induced stress granules and age-related puncta. Arrows mark colocalization of chaperones with age-related puncta. Representative single plane images. Scale bar 5μm.
(I) No significant change in tagRFP::PAB-1 aggregation with age by DNJ-19::YFP overexpression in a population of *C. elegans* at day 7 (p>0.05).
(J) KIN-19::Venus expression does not induce widespread PAB-1 stress granule formation. Scale bar 7μm.

Supplemental tables:

Table S1: Long-lived *C. elegans* with reduced insulin/IGF-1 signaling efficiently prevent protein insolubility with age. Related to Figure 1.

In category "Control RNAi aged/young" bold highlights insoluble proteins with more than 2 fold accumulation with age in control conditions. In category "*daf-2* RNAi aged/young" bold highlights proteins which aggregate with age in *daf-2(-)* conditions (>1.2 fold), underlined highlights proteins with reduced aggregation with age in *daf-2(-)* conditions (<0.83 fold).

Table S2. Functional annotation of age-dependent protein insolubility modulated by reduced *daf-2* signaling. Related to Figure 1.

(A) RNA-binding proteins are over-represented among the proteins which are protected from aggregation in the long-lived *daf-2(-)* animals

Gene ontology or SP-PIR Keyword	Number of proteins	% of total	*p* Value
Ribosomal protein	32	37.6	1.6E-39
Growth	45	52.9	3.2E-10
RNA-binding	10	11.8	6.6E-07
Muscle proteins	4	4.7	3.1E-04
Determination of adult life span	11	12.9	8.5E-04
Generation of precursor metabolites and energy	7	8.2	0.009

Functional annotation of the protein set which aggregated less with age in *daf-2(-)* conditions was carried out using the DAVID software. A total of 85 out of 87 aggregated proteins were recognized by DAVID. Enrichment in GOTERM_BP_FAT and SP_PIR_KEYWORDS were evaluated. EASE score p value: modified Fisher Exact p-value.

(B) Chaperones and yolk proteins are over-represented among proteins which are still prone to aggregate in long-lived *daf-2(-)* animals

Gene ontology or SP-PIR Keyword	Number of proteins	% of total	*p* Value
Stress response	7	14	6.4E-08
(7 Chaperones)			
Secreted	7	14	7.3E-06
(5 Vitellogenins)			
Determination of adult life span	7	14	0.002

Functional annotation of the protein set which continued to aggregate with age in *daf-2(-)* conditions was carried out using the DAVID software. A total of 50 out of 52 aggregated proteins were recognized by DAVID. Enrichment in GOTERM_BP_FAT and SP_PIR_KEYWORDS were evaluated. EASE score p value: modified Fisher Exact p-value.

Table S3. RNA-binding proteins protected from aggregation in the long-lived *daf-2(-)* animals. Related to Figure 1.

Uniprot KB	Gene name	Protein name	Prion-like domain*	Stress granule[#]	P-granule[$]
P27639	*inf-1*	Eukaryotic initiation factor 4A		yes	
P34563	*iff-1*	Eukaryotic translation initiation factor 5A-1		yes	
Q19072	*tufm-1*	Elongation factor Tu		yes	
P53013	*eft-3*	Elongation factor 1-alpha		yes	
O16520	*erfa-1*	Eukaryotic peptide chain release factor subunit 1			
Q22037	*hrp-1*	Heterogeneous nuclear ribonucleoprotein A1	yes	yes	
Q9U302	*pab-1*	Polyadenylate-binding protein	yes	yes	yes
Q9XW17	*car-1*	CAR-1	yes	yes	yes
Q9XTJ6	*cey-4*	CEY-4		yes	yes
P34689	*glh-1*	ATP-dependent RNA helicase glh-1			yes
Q22053	*fib-1*	rRNA 2'-O-methyltransferase fibrillarin	yes		

(*) RNA-binding proteins containing prion-like domains as determined by the algorithm developed by Alberti et al. 2009.

([#],[$]) RNA-binding proteins previously shown to localize to stress granules or P-granules in the literature (including references to their homologs in other organisms).

Table S4: Proteins precipitated by b-isox are prone to aggregate with age in *C. elegans* and not in long-lived *daf-2(-)* conditions. Related to Figure 1.

Table S5: Lifespan analysis of *pmyo-2::tagRFP::PAB-1* transgenics. Related to Figure 4.

Temperature	Transgenics	Mean lifespan (Days)	Age at 75% mortility (days)	Number of transgenic animals	Censored	P-value
15°C	wildtype	24.12	28	103	19	
	pmyo-2::tagRFP::PAB-1	31.44	35	100	38	<0.0001
20°C	wildtype	19.37	22	100	18	
	pmyo-2::tagRFP::PAB-1	23.62	27	101	23	<0.0001
25°C	wildtype	9.22	12	100	12	
	pmyo-2::tagRFP::PAB-1	14.06	17	99	31	<0.0001
20°C, 25°C from day 7 Repeat 1	*pmyo-2::tagRFP::PAB-1* low+medium aggregation	19.66	21	159	35	
	pmyo-2::tagRFP::PAB-1 high aggregation	18.54	21	60	4	0.029
20°C, 25°C from day 7 Repeat 2	*pmyo-2::tagRFP::PAB-1* low+medium aggregation	18.26	21	129	12	
	pmyo-2::tagRFP::PAB-1 high aggregation	18.53	21	31	5	0.562
20°C, 25°C from day 7 Repeat 3	*pmyo-2::tagRFP::PAB-1* low+medium aggregation	19.04	21	112	62	
	pmyo-2::tagRFP::PAB-1 high aggregation	15.73	17	25	2	<0.0001
20°C, 25°C from day 7 Repeat 4	*pmyo-2::tagRFP::PAB-1* low+medium aggregation	20.62	23	228	44	
	pmyo-2::tagRFP::PAB-1 high aggregation	19.42	22	89	5	0.030
20°C, sorted at day 7	*pmyo-2::tagRFP::PAB-1* low+medium aggregation	21.73	24	155	24	
	pmyo-2::tagRFP::PAB-1 high aggregation	20.64	24	89	16	0.028

Table S6: RNAi targeting of HSP-70 does not affect PAB-1 aggregation rates. Related to Figure 5.

	Repeat 1				Repeat 2			
	Day 1		Day 2		Day 1		Day 2	
Aggregation levels	Control	HSP-70	Control	HSP-70	Control	HSP-70	Control	HSP-70
Low	90	77	80	79	93	94	77	64
Intermediate	12	22	19	17	7	5	8	12
High	2	1	6	6	4	3	9	13

Number of animals with categories of tagRFP::PAB-1 aggregation: low (<10 tagRFP::PAB-1 puncta), intermediate (>10 tagRFP::PAB-1 puncta in posterior bulb), high (>10 tagRFP::PAB-1 puncta in anterior bulb). Empty vector control or RNAi targeting HSP-70 (CELE_C12C8.1).

Supplemental movies:

Movie S1. Smaller animals with PAB-1 aggregates are less motile. Related to Figure 4

Pmyo-2::tagRFP::PAB-1 animals grown at 20°C until day 7 before transfer to 25°C until day 10. Representative small (775µm) and big (1257 µm) worms were filmed at day 10.

Supplemental Experimental Procedures:

Strains:
Wild type: N2
CF2253: *gon-2(q388) I (outcrossed 4x)*
CF1041: *daf-2(e1370) III*

Transgenics:
CF3706: N2; *muEx587[Pkin-19::kin-19::mEOS2+Punc-122::gfp]*
DCD101: *hsf-1(sy441) I; daf-2(e1370) III; uqIs24[Pmyo-2::tagrfp::pab-1]*
DCD179: N2*; uqEx37[Pkin19::kin19::venus + Punc-122::gfp]*
DCD194: N2; *uqEx41[Pmyo-2::venus::tiar-2]*
DCD214: N2; *uqIs24[Pmyo-2::tagrfp::pab-1]*
DCD215: *daf-2(e1370) III; uqIs24[Pmyo-2::tagrfp::pab-1]*
DCD217: N2; *uqIs24[Pmyo-2::tagrfp::pab-1]; uqEx37[Pkin-19::kin-19::venus + Punc-122::gfp]*
DCD219: N2; *uqIs24[Pmyo-2::tagrfp::pab-1]; uqEx41[Pmyo-2::venus::tiar-2]*
DCD236: *daf-16(mu86) I; daf-2(e1370) III; uqIs24[Pmyo-2::tagrfp::pab-1]*
DCD249: *hsf-1(sy441) I; uqIs24[Pmyo-2::tagrfp::pab-1]*
DCD250: *daf-2(e1370)III; uqEx41[Pmyo-2::venus::tiar-2]*
DCD253: *eat-2(ad1116)II;uqIs24[Pmyo-2::tagrfp::pab-1]*
DCD256: *hsf-1(sy441)I; daf-2(e1370)III; uqIs24[Pmyo-2::tagrfp::pab-1]; muIs115[Phsf-1::hsf-1 + Pmyo-3::GFP]*
DCD284: N2; *uqIs24[Pmyo-2::tagrfp::pab-1]; uqEx49[pkin-19::meos]*
DCD287: N2; *uqIs24[Pmyo-2::tagrfp::pab-1]; uqIs1[pdnj-13::dnj-13::yfp]*
DCD288: N2; *uqIs24[Pmyo-2::tagrfp::pab-1]; uqIs2[pdnj-19::dnj-19::yfp]*

Maintenance:
All strains were maintained at 15°C by standard techniques on NGM plates seeded with OP50. Day 1 of adulthood is defined as 24h after the last larval stage L4. Before each experiment, adults of the desired strains were transferred to 20°C and their progeny selected at L4 stage to achieve synchronization. For experiments with worms carrying mutations as well as DCD212, DCD226, DCD194, DCD219 strains, the adults were maintained at 15°C, their progeny picked at L4 stage and thereafter transferred to 20°C.

Lifespan analysis:
Worms were grown on OP50 seeded NGM plates at the experimental temperature indicated and were scored every day for live animals, dead animals (no longer responding to body touch) and censored animals (crawled off plates, contaminated, ruptured or showing internal hatching). For lifespan analysis under mild stress, worms were grown at 20°C and transferred to 25°C at day 7. Survival analyses were performed using the Kaplan-Meier method using an online application for survival analysis (Yang et al., 2011).

Movie acquisition:
Movies were taken for 60 seconds of worms on NGM plates without bacteria using a Leica M165 FC microscope with a Planapo 2.0x objective and a Leica DFC310 FX camera. The videos were modified to play side by side at double playing speed using Vidiot software (https://sourceforge.net/projects/vidiot/).

RNAi treatment:
RNAi by feeding was performed as described previously (Hansen et al., 2005). All RNAi clones were obtained from the Marc Vidal RNAi feeding library or the Julie Ahringer RNAi feeding library (Source BioScience, UK) and sequenced. HT115 containing the empty vector L4440 was used as control.

Cloning and Strain Generation:
Cloning was carried out using the Gateway system (Life Technologies, Darmstadt, Germany). *Pmyo-2* promoter was kindly provided by Brian Lee, UCSF. *tiar-2* cDNA was amplified from a cDNA library prepared from total RNA isolated from N2 worms. The *pab-1* gene was amplified from N2 total DNA extract. All constructs contain the *unc-54* 3′ UTR. The tagrfp vector was obtained from Evrogen (AXXORA, San Diego, CA, USA). Venus was generated by targeted mutation of the *yfp* gene. Constructs were generated with fluorescent tags inserted either before or after the gene to avoid disrupting LC domain. Constructs were sequenced at each step. *Pmyo-2::tagrfp::pab-1* was injected at 10 ng/µl (whole plasmid injected), *Pkin-19::kin-19::venus* at 30ng/µl together with the coinjection marker *Punc-122::gfp* at 100ng/µl (whole plasmids injected). Undiluted PCR amplified

Pmyo-2::venus::tiar-2 was injected at 10 ng/µl to generate transgenics. All constructs were injected into N2 animals. To avoid the vector backbone, constructs were amplified by PCR with the following primers: Primer 1 (T3) ATTAACCCTCACTAAAGGGA and primer 2 TTAAGTTGGGTAACGCCAGG. Stable lines expressing PAB-1 were generated by irradiating the animals containing the extrachromosomal array in a CL-1000 Ultraviolet Crosslinker (UVP) with 275µJ x 100. 100% transmission line was backcrossed four times into the wild-type N2 strain. Non-integrated strains expressing DNJ-13::YFP and DNJ-19::YFP were obtained from Klaus Richter (Papsdorf et al., 2014) and integrated by gamma irradiation following standard procedures. These strains were then backcrossed three times into the wild-type N2 strain.

Imaging and immunofluorescence staining:
Fixation protocols for direct confocal analysis or immunohistochemistry were adapted from a fixation protocol previously described (Antibody Staining of *C. elegans* by Michael Koelle, https://medicine.yale.edu/lab/koelle/protocols/Antibody%20Staining_180540_21947.pdf). Worms at the desired age and after treatment were picked into M9 containing OP50 and then washed once with H_2O before being resuspended in fixation solution containing 1% PFA. After mixing thoroughly, worms were immediately immersed into liquid nitrogen for freezing. Tubes were thawed at 70°C and refrozen in dry ice two times and then rotated overnight at 4°C. For direct confocal analysis worms were washed hereafter with PBST-B and optionally stained with Hoechst33342 stain (NucBlue Live Cell Stain Ready Probes Reagent, Life Technologies) for 20 minutes before washing again and mounting them on slides using Fluorescent Mounting Medium (Dako). For immunohistochemistry, worms were permeabilized and stained as previously described using PAB-1 antibody (1:200, (Scheckel et al., 2012)) and AlexaFluor488 conjugated anti-rabbit (Invitrogen) diluted 1:200 as secondary antibody. Worms were stained with Hoechst33342 for 20 minutes and placed on a slide using Fluorescent Mounting Medium (Dako).
Worms were examined under a Leica SP8 confocal microscope with the HC PL APO CS2 63x1.40 oil objective using the Leica HyD hybrid detector. In single transgenics, tagRFP was detected using 555nm as excitation and an emission range from 560-650nm, Venus with 514nm as excitation wavelength and an emission range from 520-570nm. In double transgenic animals emission ranges were narrowed to 570-600nm for tagRFP and 521-551nm for Venus to prevent detection of cross-emission. Hoechst33342 staining was visualized with an excitation of 405nm and an emission range from 430-500nm. Alexa Fluor488 antibody was excited with 488nm and detected with an emission range from 500-550nm. 3D reconstructions were performed using the Leica Application Suite (LAS X). Puncta size of single plane images was determined using Fiji software (Schindelin et al., 2012).

FRAP analysis:
FRAP analysis was performed as previously described (David et al., 2010) using the Leica SP8 confocal microscope with the HC PL APO CS2 63x 1.30 glycerol objective and PMT detector. Bleach settings: 4x 20% for PAB-1 and TIAR-2 puncta. tagRFP: 555nm excitation, 565-620nm emission. Venus: 514 excitation, 521-551nm emission. Relative fluorescence intensity (RFI) was analyzed as described previously following the equation RFI = (Tt/Ct)/(T0/C0), where T0 is the intensity in the region of interest (ROI) before photobleaching; Tt, the intensity in the ROI at a defined time after photobleaching; C0, the intensity in the non-bleached part of the puncta before photobleaching; and Ct, the intensity in the non-bleached part of the puncta after bleaching (Brignull et al., 2006).

Insoluble protein extraction:
To isolate SDS-insoluble proteins for mass spectrometry analysis, we performed a sequential extraction as previously described (David et al., 2010). 350mg ground worms per treatment were solubilized in two volumes of a high salt RAB buffer (0.1 M MES, 1 mM EGTA, 0.1 mM EDTA, 0.5 mM MgSO4, 0.75 M NaCl, 0.02 M NaF, 1 mM PMSF, Roche Complete Inhibitors 2x, DNaseI and RNaseI). High-salt soluble proteins were removed by centrifugation with 20 000g, 20 minutes at 4°C. The pellet was reextracted in RAB buffer with 1 M sucrose to help remove lipids and then resuspended twice in two volumes of RIPA buffer (50 mM Tris pH 8, 150 mM NaCl, 5 mM EDTA, 0.5% SDS, 0.5% SDO, 1% NP-40, 1 mM PMSF, Roche Complete Inhibitors 1x). Detergent soluble proteins were removed by centrifugation with 20 000g, 20 minutes at 4°C. This final pellet containing highly insoluble proteins was resuspended in 200µl 70% formic acid and centrifuged at 50 000g to remove worm cuticlar debris.
To isolate insoluble proteins for western blot analysis, a simplified protocol was used where 50mg of ground animals in RAB buffer were directly resuspended in 150µl RIPA buffer. SDS-insoluble proteins were isolated by washing with RIPA buffer containing 0.5% SDS and centrifugation with 20 000g for 20 minutes at 4°C. To compare insoluble proteins collected by our method to those collected by Walther et al, we omitted SDS in the RIPA wash thus collecting both SDS-soluble and SDS-insoluble proteins after centrifugation with 500 000g for 10 minutes at 4°C as previously described (Walther et al., 2015). For both extractions, we washed the pellet

once in 100µl RIPA. Final pellets containing insoluble proteins were recovered in 75µl 8 M Urea, 2% SDS, 50 mM DTT, 50 mM Tris pH 7.4 at room temperature.

Insoluble protein extraction using *C. elegans* with gonads:
To investigate the effect of reduced *daf-2* signaling on protein insolubility in animals with gonads, 550 N2 and CF1041 worms were grown at 20°C. Worms were collected at day 1 or day 11 in RAB buffer and homogenized with the Precellys Lysing Kit (Cayman Chemical) using 1.4 mm ceramic beads. After adding the homogenate into tubes without beads and centrifugation at 20,000g for 20 minutes at 4°C, the protein extraction was performed as described in "Insoluble protein extraction". SDS was omitted in the RIPA wash and centrifugations were performed at 20,000g.

Mass spectrometry analysis:
SDS-insoluble proteins dissolved in formic acid were further processed for mass spectrometry analysis as previously described (David et al., 2010). Briefly, after dialysis, proteins were solubilized in final concentration of 8M Urea. After alkylation and reduction, samples were diluted in 150mM ammonium bicarbonate to obtain a final 2M Urea concentration. Proteins were digested by modified trypsin (Promega, Madison, WI) at 5% w/w overnight at 37°C. Peptides from young and aged animals on control and *daf-2* RNAi were labelled by 4-plex iTRAQ following the manufacturer's instructions (Applied Biosystems, Pleasanton, CA, USA). We checked that over 95% of the peptides were labelled with iTRAQ by analysing the sample on a 1-h LC-MS/MS run and searching the spectra, allowing iTRAQ as a variable modification. In order to decrease sample complexity and improve identification, peptides were separated by SCX fractionation and desalted. A total of 46 SCX fractions were collected. Individual SCX fractions were separated on a reverse phase C18 (LC Packings, Sunnyvale, CA) and the LC eluate was coupled to a micro-ionspray source attached to a QSTAR Pulsar Elite mass spectrometer (Applied Biosystems, Foster City, CA) (Trinidad et al., 2013). SCX fractions 1-20 contained relatively few peptides and were analysed by a single LC-MS analysis. To increase the coverage of peptides fractions 21-46 were analysed twice by LC-MS/MS. In the first analysis, only those ions with m/z between 375 and 600 were selected for data-dependent MS/MS, while in the second analysis, this range was between 590 and 1200 Da.
MS/MS spectra were analysed as previously described (David et al., 2010). We kept peptides that had at least one iTRAQ peak area over 25 counts. For proteins identified by one single peptide, peptides with an expectation value larger than 1E-3 were eliminated. For proteins identified by two or more peptides, we discarded peptides with an expectation value larger than 1E-2. The false positive rates were estimated by conducting the search using a concatenated database containing the original UniProt database as well as a version of each original entry where the sequence has been randomized. Using this stringent cut-off, we did not identify any decoy database proteins, indicating that the protein false discovery rate was much less than 1%. In the insoluble fractions, we detected a total of 438 proteins comparing extracts from day16/day3 old animals, 470 proteins comparing extracts from day18/day3 old animals and 492 proteins comparing extracts from day14/day3 old animals. To determine the relative level of each protein, we averaged the ratio of (peak area of sample of interest)/(sum of peak areas from all four conditions) for all peptides identified for each protein. To measure the fold change in levels of aggregation-prone proteins with age, we divided the ratio for aged control or aged *daf-2* RNAi samples by the respective ratio for young control or young *daf-2* RNAi samples. For further data analysis, we kept only proteins present in all three biological replicates and averaged their fold changes.
Calculation of correlations between fold changes in insolubility between the repeats (Figure S1A and S1B) was performed using GraphPad Prism 6 software. Data was tested for normality with D'Agostino & Pearson omnibus normality test and Spearman r correlation was calculated as several data sets did not pass the normality test.

Western blotting analysis:
The following antibodies were used: anti-PAB-1 (1:60, (Scheckel et al., 2012)), anti-HRP-1 (1:200, (Joeng et al., 2004)), anti-CAR-1 (1:400, (Boag et al., 2005)), anti-fibrillarin (1:1000, #2639, Cell Signaling), anti-HSP-90 (1:500, #4874, Cell Signaling) and anti-14-3-3 (1:5000, SC-1657, Santa Cruz Biotechnology). Bands detected by immunoblot or whole lanes detected by Sypro Ruby blot staining (Thermo Scientific) for total protein levels were quantified using Image J.

Bioinformatics analysis:
The *C. elegans* proteome set was prepared by obtaining all proteins identified by mass spectrometry available in PeptideAtlas 2011 (http://www.peptideatlas.org) with a PeptideProphet probability over 0.9. Proteins identified in our experiment but not in the PeptideAtlas database were added to this proteome set (final total: 7454 proteins). To exclude possible biases in sequence or structural properties due to the presence of transmembrane helices, we removed all proteins predicted to contain transmembrane helices using TMHMM v2.0 (Krogh et al., 2001), resulting in 6102 proteins. To prevent bias due to redundancy, we reduced the sequence identity of the set

to 50% using CD-HIT v3.1.1 (Li and Godzik, 2006), resulting in 5637 proteins. These procedures were also applied to our aggregation-prone set and the published set of proteins precipitated by b-isox from U2OS cells. Functional annotation of the aggregation-prone set was done using the freely available DAVID software (http://david.abcc.ncifcrf.gov/). The *C. elegans* proteome set of mass spectrometry detectable proteins was chosen as the background list. GOTERM_BP_FAT and SP_PIR_KEYWORDS were used for the analysis. Redundant categories were removed using the functional annotation clustering option.

Supplemental References:

Boag, P.R., Nakamura, A., and Blackwell, T.K. (2005). A conserved RNA-protein complex component involved in physiological germline apoptosis regulation in C. elegans. Development *132*, 4975-4986.

Brignull, H.R., Morley, J.F., Garcia, S.M., and Morimoto, R.I. (2006). Modeling polyglutamine pathogenesis in C. elegans. Methods in enzymology *412*, 256-282.

David, D.C., Ollikainen, N., Trinidad, J.C., Cary, M.P., Burlingame, A.L., and Kenyon, C. (2010). Widespread protein aggregation as an inherent part of aging in C. elegans. PLoS biology *8*, e1000450.

Hansen, M., Hsu, A.L., Dillin, A., and Kenyon, C. (2005). New genes tied to endocrine, metabolic, and dietary regulation of lifespan from a Caenorhabditis elegans genomic RNAi screen. PLoS Genet *1*, 119-128.

Joeng, K.S., Song, E.J., Lee, K.J., and Lee, J. (2004). Long lifespan in worms with long telomeric DNA. Nature genetics *36*, 607-611.

Krogh, A., Larsson, B., von Heijne, G., and Sonnhammer, E.L. (2001). Predicting transmembrane protein topology with a hidden Markov model: application to complete genomes. Journal of molecular biology *305*, 567-580.

Li, W., and Godzik, A. (2006). Cd-hit: a fast program for clustering and comparing large sets of protein or nucleotide sequences. Bioinformatics *22*, 1658-1659.

Papsdorf, K., Sacherl, J., and Richter, K. (2014). The balanced regulation of Hsc70 by DNJ-13 and UNC-23 is required for muscle functionality. The Journal of biological chemistry *289*, 25250-25261.

Scheckel, C., Gaidatzis, D., Wright, J.E., and Ciosk, R. (2012). Genome-wide analysis of GLD-1-mediated mRNA regulation suggests a role in mRNA storage. PLoS Genet *8*, e1002742.

Schindelin, J., Arganda-Carreras, I., Frise, E., Kaynig, V., Longair, M., Pietzsch, T., Preibisch, S., Rueden, C., Saalfeld, S., Schmid, B., *et al.* (2012). Fiji: an open-source platform for biological-image analysis. Nat Methods *9*, 676-682.

Trinidad, J.C., Thalhammer, A., Burlingame, A.L., and Schoepfer, R. (2013). Activity-dependent protein dynamics define interconnected cores of co-regulated postsynaptic proteins. Molecular & cellular proteomics : MCP *12*, 29-41.

Walther, D.M., Kasturi, P., Zheng, M., Pinkert, S., Vecchi, G., Ciryam, P., Morimoto, R.I., Dobson, C.M., Vendruscolo, M., Mann, M., *et al.* (2015). Widespread Proteome Remodeling and Aggregation in Aging C. elegans. Cell *161*, 919-932.

Yang, J.S., Nam, H.J., Seo, M., Han, S.K., Choi, Y., Nam, H.G., Lee, S.J., and Kim, S. (2011). OASIS: online application for the survival analysis of lifespan assays performed in aging research. PloS one *6*, e23525.